UNESCO Chair on
Coastal Geo-Hazard Analysis
Research Institute for Earth Sciences
Geological Survey of Iran
unesco
Chair

Abstract

The Alborz Mountain range, stretching 600 km in length, 70–130 km in width, and rising up to 3500–4000 m, divides the South Caspian Basin to the north from the Great Kavir Basin to the south. Its parallel folds and thrust faults arise from the convergence of Central Iran and Eurasia. Current regional kinematics feature strain partitioning, characterized by left-lateral strike-slip faulting along the range's inner section and reverse faulting at its borders. To the north, the South Caspian Basin meets Eurasia at a subduction zone (Apsheron sill) traversing the central Caspian Sea and is believed to be rotating clockwise. GPS measurements and slip-rate data indicate that the northern Alborz margin, near the Khazar Fault, absorbs much of the present shortening between the South Caspian and Great Kavir basins, although the Khazar Fault's characteristics are not well documented. Morphotectonic and paleoseismological studies reveal the Khazar Fault as the most rapidly moving active fault in the Alborz range, capable of producing earthquakes of magnitude 7 or greater.

ISBN : 978-622-8423-19-7

9 786228 423197

2024

UNESCO Chair on
Coastal Geo-Hazard Analysis
Research Institute for Earth Sciences
Geological Survey of Iran
unesco
Chair

Geometry, kinematics, and archaeoseismology of the Khazar Fault System in Northern Iran, the southern Caspian Sea

UCCGHA 025

2024

Geometry, kinematics, and archaeoseismology of the Khazar Fault System in Northern Iran, the southern Caspian Sea

Geometry, kinematics, and archaeoseismology of the Khazar Fault System in Northern Iran, the southern Caspian Sea

Author:

Hamid Nazari, Negar Haghipour, Mehdi Mohammadi Vizheh

نشرخزه

UNESCO Chair on Coastal Geo-Hazard Analysis
Research Institute for Earth Sciences
Geological Survey of Iran
unesco Chair
نشر خزه

اطلاعات گزارش

عنوان: ژئومتری، کینماتیک و زمین‌باستان‌شناسی سامانه گسل خزر در شمال ایران، جنوب دریای کاسپین

مجری: پژوهشکده علوم زمین، آزمایشگاه علوم زمین مونپلیه، دانشگاه مونپلیه، سازمان زمین‌شناسی

زبان مرجع: انگلیسی - فارسی

خروجی: گزارش، نقشه، مقاله، داده‌های الکترونیکی

ناظران علمی: حمید نظری

نویسندگان: حمید نظری، ژان فرانسوا ریتز، ژان پیر بورگ، نگار حقی‌پور، محمدعلی شکری، محمدرضا انسانی، مهدی محمدی ویژه، آرا آوگیان، حسن فاضلی نشلی

رئیس کرسی یونسکو در مخاطرات زمین شناختی ساحلی: حمید نظری

مسئول شورای اجرایی: راضیه لک

خلاصه‌نویسی و ترجمه به انگلیسی: منوچهر قرشی

ناشر: نشر خزه

با همکاری کرسی یونسکو در مخاطرات زمین شناختی ساحلی

چاپ اول: ۱۴۰۳

شمارگان: ۵۰ نسخه

صفحات: ۸۸

شابک: ۷-۱۹-۸۴۲۳-۶۲۲-۹۷۸

khazepub@gmail.com

Report Information

Title: Geometry, kinematics, and archaeoseismology of the Khazar Fault System in Northern Iran, the southern Caspian Sea

Employer: Research Institute for Earth Sciences, Laboratoire Géosciences Montpellier, Université de Montpellier, Geological Survey of Iran

Original language: English - Persian

Output: Report, Map, Paper, Digital Meta Data

Supervisors: Hamid Nazari

Authors: Hamid Nazari, Jean-Francois Ritz, Jean-Pierre Burg, Negar Haghipour, Mohamadali Shokri, Mohamadreza Ensani, Mehdi Mohammadi Vizheh, Ara Avagyan, Hasan Fazeli Nashli

Chairholder in the UNESCO Chair on Coastal Geo-Hazard Analysis: Hamid Nazari

Head of the Executive Council: Razyeh Lak

Summarized and translated into English: Manouchehr Ghorashi

Publisher: Khazeh Publication

with cooperation UNESCO Chair on Coastal Geo-Hazard Analysis

First Edition: 2024

Edition number: 50

Page: 88

Shabak: 978-622-8423-19-7

khazepub@gmail.com

Scientific Council	
Name	**Affiliation**
Behrouz Abtahi	Shahid Beheshti University (SBU)
Philippe Agard	University of Sorbonne
Justin Ahanhanzo	Intergovernmental Oceanographic Commission of UNESCO (IOC-UNESCO)
Hamid Alizadeh Lahijani	Iranian National Institute for Oceanography and Atmospheric Science
Ryo Anma	Tokushima University
Franck A. Audemard	Department of Geology, Central University of Venezuela
Alice Aurelie	UNESCO Water Sciences Division
Ara Avagyan	IGS: Institute Geological Sciences
Yeong Bae Seong	Korea University
Rick J Bailey	IOC-UNESCO Indian Ocean Tsunami Warning and Mitigation System/ UNESCO
Abbas Banj Shafiei	Urmia University
Eric Barrier	University of Sorbonne
Yahya Djamour	Shahid Beheshti University (SBU)
Issa El-Hussain	Sultan Qaboos University
Aram Fathian Baneh	University of Calgary
Hassan Fazeli Nashli	University of Tehran
Magdi Guirguis	Institut français d’archéologie orientale du Caire
Martin Hanz	German under water archaeology association

Ekkehard Holzbecher	German University of Technology in Oman
Egor Krasinskiy	Underwater research center Russian Geographical Society
Razyeh Lak	Research Institute for Earth Sciences
John Lambert	Deltares, UNESCO
Mohammad Mokhtari	International Institute of Earthquake Engineering and Seismology
Hamid Nazari	Research Institute for Earth Sciences
Jafar Omrani	Geological Survey of Iran
Klaus Reicherter	Aachen University
Jean-François Ritz	University of Montpellier
Stefano Salvi	National Institute of Geophysics and Volcanology (INGV)
Morteza Talebian	Research Institute for Earth Sciences
Mohammad Tatar	International Institute of Earthquake Engineering and Seismology
Judith Thomalsky	German Archaeological Institute Tehran Branch
Richard Walker	University of Oxford
Wenjiao Xiao	Chinese Academy of Sciences
Alireza Zarasvandi	Iranian Research Organization for Science & Technology (IROST) – Ministry of Science, Research & Technology
Mahdi Zare	International Institute of Earthquake Engineering and Seismology

Executive Committee	
Name	**Affiliation**
Nasir Ahmadi	Environmental Protection Organization of Mazandaran Province
Arash Amini	Golestan University
Alireza Amrikazemi	Scientific Coordinator, Qeshm Island UNESCO Global Geopark
Parviz Armani	Imam Khomeini International University
Ataollah Dadashpour	Geological Survey of Iran, Sari branch
Asghar Dolati	Kharazmi University
Hasan Fazelinashli	University of Tehran
Fahimeh Foroghi	Iranian National Institute for Oceanography and Atmospheric Science
Abdolazaim Ghanghormeh	Golestan University
Habibolah Ghasemi	Shahrood University of Technology
Mohammad reza Ghasemi	Research Institute for Earth Sciences
Manouchehr Ghorashi	Research Institute for Earth Sciences
Ahmed Hadidi	German University of Technology in Oman (GUTECH)
Jafar Hassanpour	University of Tehran
Ataollah Kavian	Environmental Protection Organization of Mazandaran Province
Razyeh Lak	Head of RIES and Executive Manager
Mahmoudreza Majidifard	Research Institute for Earth Sciences
Majid Moghadam	Iranian Research Organization for Science &

	Technology (IROST)
Ali Akbar Momeni	Shahrood University of Technology
Babak Moradi	Iranian National Institute for Oceanography and Atmospheric Science
Seyed Mohsen Mortazavi	Hormozgan University
Hasan Nasrollah Zadeh	Caspian Sea Ecological Research Center
Ehsan Pegah	Kharazmi University
Abdolwahed Pehpouri	Qeshm Island UNESCO Global Geopark
Ahmadreza Rabani	University of Science and Technology of Mazandaran
Mahdi Rahmanian	Shargh Daily newspaper
Ahmad Rashidi	International Institute of Earthquake Engineering and Seismology
Masoud Sadri Nasab	University of Tehran
Mohammad Tatar	International Institute of Earthquake Engineering and Seismology
Alireza Vaezi	Research Institute for Earth Sciences
Mojtaba Yamani	University of Tehran
Secretariat	
Name	**Affiliation**
Elnaz Aghaali	Research Institute for Earth Sciences
Keivan Ajdari	Research Institute for Earth Sciences
Hourieh AliBeygi	Research Institute for Earth Sciences
Bahman Bahrami	Memaran Asr Ertebat Company
Hanieh Bakhshaei	Geological Survey of Iran

Reza Behbahani	Geological Survey of Iran
Javad Darvishi khatooni	Geological Survey of Iran
Mohammadreza Ensani	Geological Survey of Iran
Marziyeh Estrabi Ashtiyani	Geological Survey of Iran
Sedigheh Ghanipour	Research Institute for Earth Sciences
Elaheh Ghayoumi	Memaran Asr Ertebat Company
Gholamreza Hoseinyar	Geological Survey of Iran
Mojtaba Kavianpour Sangno	Geological Survey of Iran
Zeinab Kazeminia	Research Institute for Earth Sciences
Hamoon Memarian	Research Institute for Earth Sciences
Mehrnoosh Pour Saeid	Graphic Designer
Shirin Safavi	Research Institute for Earth Sciences
Aazam Takhtchin	Research Institute for Earth Sciences

Contents

Table of Figures

Grayish brown silts and clays, a few clasts (1–3 mm), pieces of pottery, stone tools, brick color patches (1 mm-10 cm) more than in units 1–4, consolidated, in some parts thin layers of carbonate, sporadic charcoals and chunks of bones (animal?), chalk (thickness 3–7 cm) in the lower part. U6: Gray lens of silts and clays, (10–15% clasts (2 mm-1 cm, rarely 3 cm), non-stratified, angular to subangular, abundant pieces of charcoal, pieces of pottery bones (animal?) and teeth (human?), brick color patches (2 mm-3 cm), a piece of brick 5 cm6cm. U7: Gray lens of silts, 10–15% clast (2–5 mm), sorted, patches brick color (2–3 mm, up to 1 cm), pieces of pottery in base (7–1 0 cm), interlayers of chalk (thickness 1 cm), charcoals and chunks of bones, non-stratified, similar to unit 6. U8: Grayish buff, alternating of thin layers of silts and carbonaceous (3–4 cm), stratified, less 5% clast (1–3 mm up to 5 mm), pieces of pottery (1–8 cm), patches brick color (5 mm-5 cm), loose to moderate hardness. U9: Grey silts and clays, a few clasts (1–3 mm), pieces of pottery (rarely 8 cm), patches brick color (2 mm-30 cm), the thick brick color 4 cm in the top, charcoals, thin layer of charcoal at the base in the northern part, sporadic fractures, similar to units 6,7 and 8. U10: Light brown silts and clays, 5–10% clast (1–5 mm, rarely 1–2 cm), sub-rounded, abundant brick color patches (2–4 mm, up to 1-3cmm), pieces of pottery (1–7 cm), pieces of bones, sporadic chunks of charcoal, medium compaction, non-stratified (flood plain/lagoon deposits). U11: Non-situ, gray silts, and ashes (peat?), without clast, sporadic charcoals increasing at the base of the unit, brick color patches (6–12 cm), loose (flood plain deposits). U12: Gray lens, alternating layers of silts and carbonates (ashes?), without clast, patches brick color (0.5–3 cm), pieces of pottery (1–2 cm up to 10–12 cm), a few chunks of charcoal, loose, carbonaceous in the upper and lower part, silty in the central part, moderate compaction, like in unit 11. U13: Cream to buff silts and clays, 5–10% clast (2 mm-lcm), a few patches brick color (0.5–1 cm), pieces of pottery (1–3 cm, rarely 7 cm), subrounded, weakly stratified, alluvium deposits? U14: Separate in unit 10, brick color, abundant patches brick (2 mm-lcm), carbonaceous in northern part at the top of the unit. U15: Cream to brown silts and clays, 3–5% clast (2–5 mm) decreases to the north, pieces of pottery, patches brick color (2–3 cm), the thin layer of brick in the northern part (thickness 5 cm), pieces of bones, moderate compaction, non-stratified (flood plain/ lagoon deposits). U15a: similar but looser than U14. U15b: Cream to brick, 2–3% clast (2–3 mm up to 2 cm), pieces of pottery, charcoal, consolidated (in the southern part) which decrease in the northern part, weakly stratified (flood plain/ lagoon deposits). U16: Grey to buff, 5% clast (2 mm-l cm, rarely 3–5 cm), a few pieces of pottery, patches brick (0.5–2 cm), a few charcoals, loose compaction, weakly laminated, root print in some part (flood plain/ lagoon deposits). U17: Layers of carbonates and silts, without clast, loose, roots residual, non-stratified. U18: thin carbonate layer. U19: cream to brown, 1% clasts (2–3 mm), a few pieces of pottery, loose, non- stratified, ground surface with residual of roots and erosional channel. Log 2: U1: Light brown silts and clays, ≤3% clast (2–5 mm rarely to 2 cm), pieces of pottery in some part, contain thin layers of chalk, charcoals, compact, weakly stratified (flood plain deposits). U2: Cream silty layer, non-stratified, contain pottery crumbs, 2 pieces of stone (15–25 cm), similar to handmade soil. U3: Light brown to cream silts and clays, none stratified, consolidated, ≤3% clast, pieces of pottery, a charcoal layer at the base of unit mostly in the northern part, a thin layer of chalk in the lower part, root print in the southern part. U4: Light creamy silts, non-clear stratified, 2–5% clast (2 mm-5 mm, rarely 1.5–2 cm), pieces

Table of Table

PART I

1-1- Introduction

The Alborz Mountain range, stretching 600 km in length, 70–130 km in width, and rising up to 3500–4000 m, divides the South Caspian Basin to the north from the Great Kavir Basin to the south. Its parallel folds and thrust faults arise from the convergence of Central Iran and Eurasia. Current regional kinematics feature strain partitioning, characterized by left-lateral strike-slip faulting along the range's inner section and reverse faulting at its borders. To the north, the South Caspian Basin meets Eurasia at a subduction zone (Apsheron sill) traversing the central Caspian Sea and is believed to be rotating clockwise. GPS measurements and slip-rate data indicate that the northern Alborz margin, near the Khazar Fault, absorbs much of the present shortening between the South Caspian and Great Kavir basins, although the Khazar Fault's characteristics are not well documented. Morphotectonic and paleoseismological studies reveal the Khazar Fault as the most rapidly moving active fault in the Alborz range, capable of producing earthquakes of magnitude 7 or greater.

The south-dipping Khazar Fault may also cause relatively deep earthquakes, such as the 2004 Baladeh earthquake at depths of 20 to 30 km. It represents a significant seismic hazard for the densely populated

Caspian coast and major cities, including Tehran, on the southern Alborz piedmont. The tectonic complexity of the Alborz region is further accentuated by its interplay with numerous other geological features, such as the extensive series of thrust faults and the presence of secondary faults that actively accommodate deformation. The interplay of these structures is crucial for understanding seismic risks, as they may interact in ways that either amplify or mitigate earthquake frequencies and magnitudes. Recent seismological investigations have begun to unravel the history of the Khazar Fault, revealing a pattern of recurrent seismic events that suggest a potentially devastating cycle. In particular, paleoseismological data suggests that the Khazar Fault has produced major earthquakes approximately every 200 to 400 years, implying a pressing risk for future seismic activity. Such insights underline the necessity for ongoing monitoring and research initiatives, aimed at enhancing the earthquake preparedness of urban centers bordering the fault, particularly Tehran. The urban population, exceeding 8 million, is situated perilously close to this seismic boundary, where ground shaking could result in widespread infrastructural and human loss.

Additionally, the impact of regional and global climate change may exacerbate the existing hazards. Alterations in hydrology and temperature can influence landslide susceptibility in the steep terrains of the Alborz, while changes in precipitation patterns may affect the stability of slopes already burdened by tectonic forces. Given the mountainous topography and the increasing human activity in these areas, land use planning must integrate geological risk assessments to mitigate disaster potentials.Considering these complexities, it is imperative to establish comprehensive disaster response frameworks that incorporate both scientific knowledge and community preparedness initiatives. Public awareness campaigns, combined with robust building codes and emergency response plans, could significantly enhance resilience against natural calamities. Furthermore, interdisciplinary collaborations among geologists, urban planners, and policymakers are essential to foster sustainable development while maintaining vigilance against the inherent geological threats posed by the active tectonic landscape of the Alborz Mountain range.1-2- Tectonic setting

The Alborz Mountains have recorded several orogenies from late Precambrian-early Paleozoic to Neogene times (Berberian and King, 1981; Alavi, 1996; Allen et al., 2003). It is a crustal-scale flower structure with a double-verging fold-and-thrust system both to the north and to the south (Stöcklin, 1974; Allen et al., 2003, Nazari, 2006; Ritz et al., 2006, Guest et al., 2006, Shahidi, 2008, Nazari and Ritz, 2008) (Figure 1).

At present, the Alborz Mountains experience transpression associated with the mostly NS motion of Central Iran towards the South Caspian Basin (Jackson et al., 2002). This motion is associated with the clockwise rotation of the South Caspian relative to Eurasia (Jackson et al., 2002; Allen et al., 2003; Ritz, 2006), which is consistent with a fault-block model computed from GPS data (Vernant et al., 2004; Djamour et al., 2010). The debated age of the onset of the South Caspian motion with respect to stable Eurasia varies between 1 and 10 Ma (see Allen et al., 2003; Ritz et al., 2006; Hollingworth et al., 2008). This relatively wide range depends on the models used by different authors. Ritz (2009) proposed an integrating scenario in which the South Caspian Basin started moving north relative to Eurasia, subducting below the Apsheron Sill between 10 and 5 Ma, and then acquired a clockwise rotational motion in the Pleistocene (1–2 Ma). This interpretation is compatible with: (1) the maximum depth of about 60–80 km for earthquakes beneath the Apsheron Sill (Jackson et al., 2002); this depth would be reached within ~ 10 Myr by the South Caspian subducting slab at the present-day convergence rate of ~ 6 mm/yr (Vernant et al., 2004); (2) the estimated ~ 35 km of WNW-ESE along-strike extension of the Kopeh Dagh, the mountain range which extends the Alborz to the east of the Caspian Sea, would require ~ 10 Myr at the present-day GPS rate of 2–3 mm/yr (Hollingsworth et al., 2008); and (3) the cumulative displacement of ~ 3–5 km along the present left-lateral strike-slip faults of the inner Alborz, which would require 1–2 Ma at the present-day slip rates of 2–3 mm/yr (Vernant et al., 2004; Ritz et al., 2006; Nazari et al., 2014). The Khazar Fault is defined as a 600 km long thrust fault, placing the Mesozoic and Neogene rocks of the northern Alborz over the 20-km- thick Neogene and Quaternary deposits of the South Caspian Basin (Ghassemi, 2005; Nazari et al., 2005; Brunet et al., 2003; Rashidi, 2021). Its surface expression follows the major break of slope separating the Alborz foothills from the undeformed flat area along the southern shoreline of the Caspian Sea (Nazari, 2006, 2015). This feature is clear in the western Alborz, whereas the fault is usually hidden, segmented, and expressed as fault-propagation folds in the eastern Alborz (Ghassemi, 2005).

Several historical earthquakes have been attributed to the Khazar Fault: e.g., at Amol 1809 BCE, 1224 CE; Polrud-Tonekabon 1485 CE; Rudsar 1400 CE; Lahijan 1678 CE; Rasht 1709, 1713, 1854, 1857 CE; and Rasht-Anzali-Shemaka 1854 (Ambraseys and Melville, 1982; Berberian et al., 1992; Berberian, 1996; see blue diamonds in Figure 1). In reality, there is no firm evidence for their association with any particular fault. The 2004 (M 6.4) Baladeh earthquake (Tatar et al., 2007), is the last large earthquake to have occurred in Alborz after the 1957 (M7.1) Sangechal event, about 80 90 km further east. Local and teleseismic data for the Baladeh earthquake allow a convincing association with the Khazar Fault (Tatar et al., 2007). There was no surface rupture for this event, not surprisingly as it and its aftershocks were mostly at depths of –30 km; but its well-determined reverse-fault mechanism, hypocenter, and south-dipping aftershock zone indicate that the causative fault projects to the surface at the expected location of the Khazar Fault. The data for the 1957 earthquake are poor, though its focal mechanism was probably similar to that of the 2004 Baladeh event (McKenzie, 1972). Tatar et al., (2007) argue that it, too, could have occurred on the Khazar Fault.

Djamour et al., (2010) calculated a fault-block model from GPS data, in which the Khazar Fault is one of the main active structures in the Alborz Mountains. In its western segment, the fault absorbs a shortening of ~ 6 mm/yr with a left-lateral component of 1.8 mm/yr, whereas in its eastern section, motion is principally left-lateral strike-slip at ~ 5 mm/yr with minor shortening of 2–3 mm/yr (the authors specify that these are maximum rates with uncertainties of ~ 2 mm/yr). These geological, seismological, and geodetic observations raise the question of whether the co-seismic earthquake rupture on the active Khazar Fault ever reached the ground surface. Tatar et al., (2007) suggest that it may be aseismic at shallow levels, because of the large thickness of overridden weak Caspian sediments. There is a need to know better its long-term geological slip rate in the Late Quaternary, as well as the likely recurrence interval for large earthquakes.

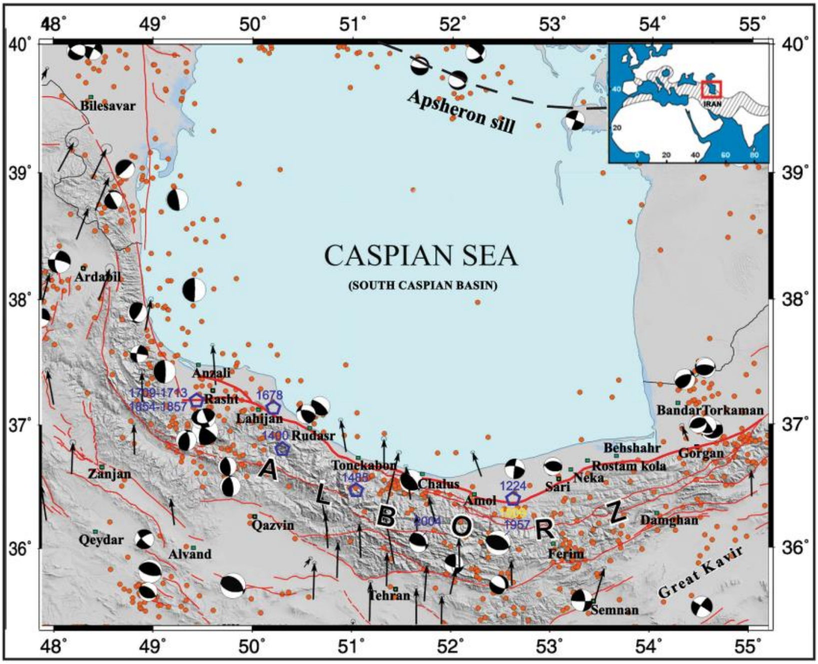

Figure 1: Seismotectonic sketch map of the South Caspian region (modified after Talebian et al., 2013). The dashed thin and thick red lines represent inferred minor and major faults. The thick red line defines the Khazar Fault on the northern flank of the Alborz Mountain range. Earthquake focal mechanisms are summarized from Jackson et al., (2002), Tatar et al., (2007), and the global CMT catalog. All instrumentally documented earthquakes in the Alborz are shallower than about 35 km. orange dots show epicenters of earthquakes with Mw> 5 (Engdahl et al., 1998; Engdahl and Villase˜ nor, 2002). Diamonds with dates represent historical earthquakes that may be associated with the Khazar Fault, after Berberian et al., 1992 and Berberian 1996 (white event AD, yellow event BC). Black arrows are GPS velocity vectors (in mm/yr) relative to Eurasia (http://www.ncc.ir).

1-2- Morphotectonic analysis

1-2-1- General geomorphology of the Khazar fault

The Khazar Fault is identified as an active thrust on the 1:250,000 neotectonic and seismotectonic maps by the Geological Survey of Iran, stretching along the northern front of the Alborz Mountains from Rasht (49.5°E) to Gonbad-e Qabus (55.2°E) (Figure 1). Although dense vegetation obscures the northern slopes, the Khazar Fault, referred to as a hidden fault (Nazari et al., 2005; Nazari, 2006), is evident as a slope break between foothills and the flat coastal plain. The WNW-ESE trending topographic scarp extends continuously from longitude 50.00°E (Lahijan) to 52.5°E (southeast of Amol) (Figure 2a). Between 52.5°E and 53.3°E (Nek`a), the ridges defining the slope break are oblique to the main trend, indicating fault segmentation. From 53.5°E to 54.3°E (Gorgan), an EW-trending section presents topographic scarps aligned with the principal slope break. However, east of Gorgan, where the Alborz ranges ENE-WSW, there is no geomorphological evidence of recent fault activity.

Topographic profiles, derived from a 1:50,000 Digital Model (DEM), show the altitude of the Khazar Fault's main slope break varies between 20 and 200 m (Figure 2b). This variation suggests it is not a shoreline feature, despite some paleo-shoreline influences at lower elevations (Brookfield and Hashmat, 2001; Guest et al., 2006). In the DEM's western section, the fault is clearly defined at the main relief's base (profiles P8 - P4), while in the east, it bounds a zone of low relief in front of the mountain front (profiles P3 – P1; Figure 3a). These features are recognized as ‘foreberg’ structures in the literature (e.g., Bayasgalan et al., 1999; Ritz et al., 2003; Walker et al., 2003), similar to those observed in the alluvial piedmont of the southern Alborz foothills, where Tehran is situated (Ritz et al., 2012; Talebian et al., 2016). Recent studies have highlighted the significance of the Khazar Fault not only in terms of its geological characteristics but also concerning the broader tectonic framework of the region. The ongoing convergence between the Arabian and Eurasian plates plays a crucial role in the fault's dynamics, resulting in localized compressional forces that manifest through various geomorphic features. These features, which include compressional ridges and asymmetric valleys, further underline the fault's influence on the landscape.

Field investigations and GPS measurements have begun to quantify the slip rates along the fault. Preliminary results suggest a moderate slip rate, which underscores its potential to generate significant seismic events. The Khazar Fault's capacity for producing large earthquakes has implications for urban centers like Rasht and Gorgan, where population density and infrastructure development render such cities particularly vulnerable.

Additionally, the interaction of the Khazar Fault with adjacent structures, such as the Alborz range's thrust systems, raises questions about the complexity of stress transfer mechanisms within this tectonically active region. In particular, the segmentation observed between key longitudes on the fault indicates that different segments may behave independently, which complicates predictions regarding future seismic activity.

Further elucidation of the Khazar Fault's role in landscape evolution is evident through paleoseismic studies that investigate past earthquake events. By identifying and dating sedimentary layers displaced by fault activity, researchers can construct a clearer picture of the fault's seismic history. Such studies could reveal intervals of heightened activity, which can be vital for understanding the cyclic nature of stress accumulation and release in this active tectonic setting.

As new data emerges, the imperative for comprehensive hazard assessments and the implementation of mitigation strategies becomes even more pressing. The integration of geospatial technologies and community awareness programs could enhance preparedness and resilience in regions impacted by the Khazar Fault, supporting both scientific inquiry and public safety initiatives. Ongoing collaborations between geologists, seismologists, and urban planners will be essential to navigate the challenges posed by the geological complexities of northern Iran.

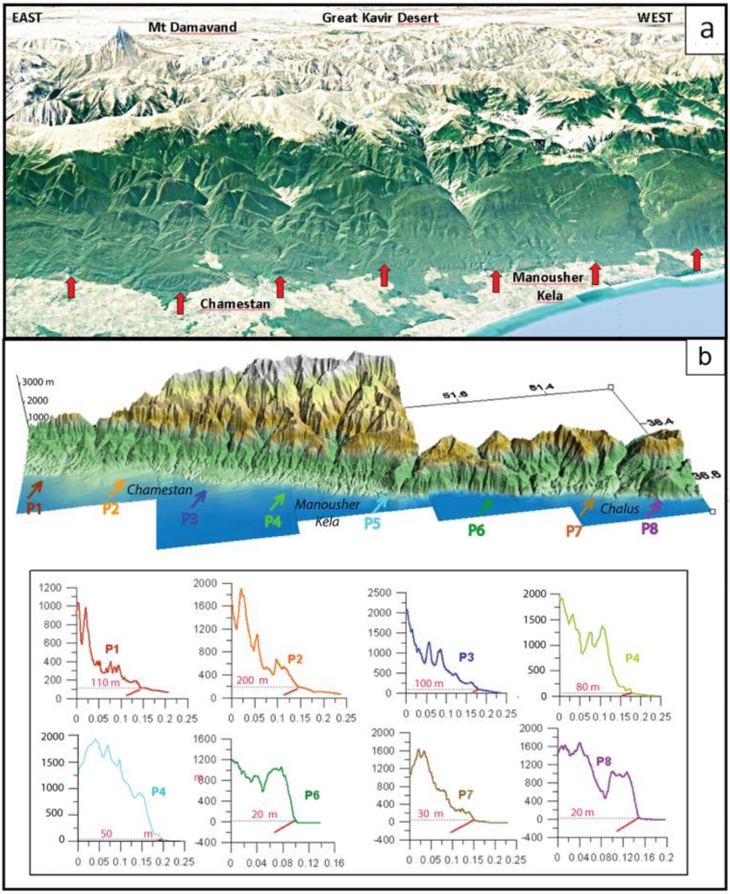

Figure 2: (a) Southwards Google Earth view of the middle part of the Alborz Mountain range (red arrows point out the topographical scarp associated with the Khazar Fault scarp; (b) 3D view of a Digital Elevation Model obtained from 1:50,000 between Amol and Chalus cities, with 8 topographic profiles indicating the altitude of the scarp associated with the Khazar Fault. (For interpretation of the references to color in this figure legend, the reader is referred to the web version of this article.)

Forebergs are fault-bend and fault-propagation folds (Bayasgalan et al., 1999) controlled by shallow thrust faults reaching a few kilometers in front of the main relief and connected at depth with the main deep-seated thrust fault (Figure 3b). The foreberg morphology is related to changes in the dip of the underlying thrust fault near the surface. In some cases, the shallow thrust fault controlling the foreberg is emergent (e.g., Prentice et al., 2002; Ritz et al., 2003), but in many cases, the fault remains buried and hidden, as is the case for the Pardisan foreberg across the Tehran city (Talebian et al., 2016). Foreberg structures generally have a limited lateral extent of 5–20 km and are not found in the foothills of all mountain range-fronts. The Chamestan Foreberg shown in Fig. 3a extends over a length of ~ 10 km. The morphology of the relief on either side of the foreberg suggests that the Khazar Fault dips 30° to 45° to the south (Figure 3c).

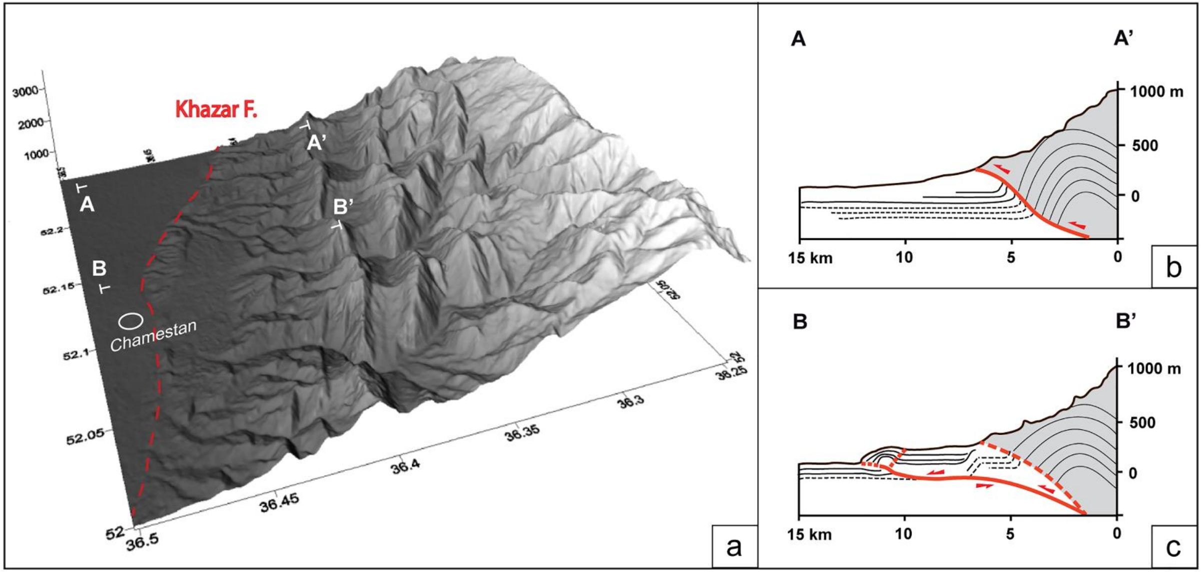

Figure 3: (a) Oblique view of a section of the DEM between longitudes E52° and E52.25° (around Chamestan city) showing the topographic scarp associated with the Khazar Fault; (b) Simplified cross-section within the main mountain front; (c): Simplified cross-section within a fault-propagation fold (foreberg structure) in front of the main mountain front.

1-2-2- Estimating the long-term slip rate, the magnitude, and the recurrence intervals for the largest events

Slip rate - It is difficult to determine the long-term slip rate along the Khazar Fault because both the dense forest cover and the intense human activity (e.g; rice fields, quarries, villages) have in many places modified the original geomorphology. However, a few geomorphologic markers can be used to investigate the tectonic activity of the fault. One of these, within the central section of the fault, 20 km west of Chamestan near the village of Manuchehrkola (Figure 4a), corresponds to an uplifted alluvial surface slightly tilted (≤10◦) to the south and capping older alluvium (Figure 4b). The older alluvium is strongly tilted (~50˚) towards the north in the riverbed and along a road located a little further west (Figure 4c). Similarly tilted alluvial units at several other places along the main break of the slope where inferred the Khazar Fault to be located. Based on the such observations it may conclude that the Khazar Fault often does not reach the surface.

The analysis of several topographic profiles from the uplifted alluvial surface in the hanging wall of the Khazar Fault to the footwall alluvial plain shows a vertical separation of 42 to 70 m (Figure 4d). This corresponds to the minimum vertical offset associated with thrusting along the fault, given that it remains hidden below the hangingwall alluvium. On top of the uplifted fluvial surface, a bulk sample collected (IR19-2B, Figure 4a) from a depth of 3.8 m into a thick silty unit capping the older alluvium deposits. This bulk sample was rich in organic material and gave a calibrated ^{14}C age of 28,085 ± 262 yrs BP (Table 1). Dividing the minimum vertical offset of the abandoned terrace (56 ±14 m) by this age yields a minimum vertical slip rate of 2.0 ± 0.5 mm/yr.

To estimate the minimum horizontal slip rate component (i.e., a minimum shortening rate) and the minimum slip rate along the fault itself, a SW dip of 34°, considered as determined by Tatar et.al; (2007) from teleseismic waveform analysis of the 2004 Mw 6.4 Baladeh earthquake. Dividing the minimum vertical slip rate by tangent 34° yields a minimum horizontal (shortening) slip rate of 3 mm/yr. Dividing the minimum vertical slip rate by sinus 34° yields a minimum slip rate along the Khazar Fault of 3.6 mm/yr.

Moment Magnitude of the largest events - The morphological scarp along the Khazar Fault zone shows its capacity for affecting the near-surface or rupturing the surface itself sometimes. Considering that ruptures have the same centroid depth (22 km) and the same dip (34°) as the 2004 Baladeh earthquake (Tatar et al., 2007) allows estimating a down dip rupture width of 45 ±17 km. Using Wells and Coppersmith (1994) regression law (i.e., Mw = (4.37±0.16) +(1.95 ±0.15) ×log (RW)) expressing the Moment magnitude (Mw) with respect to the down-dip rupture width (RW), we estimate that the

Khazar Fault is capable of producing events with Mw between 7.0 and 8.2. This result is consistent with the estimate of the Moment magnitude using Wells and Coppersmith (1994) regression law (Mw = (5.00 ±0.22) +(1.22 ±0.16) ×log (SRL) expressing the Moment magnitude (Mw) with respect to the surface rupture length (SRL) for reverse faults. Indeed, considering a surface rupture length of 230 km (which corresponds to the length of the continuous topographic scarp between Lahijan and 52.5°E Amol; see above) yields an Mw between 7.3 and 8.5.

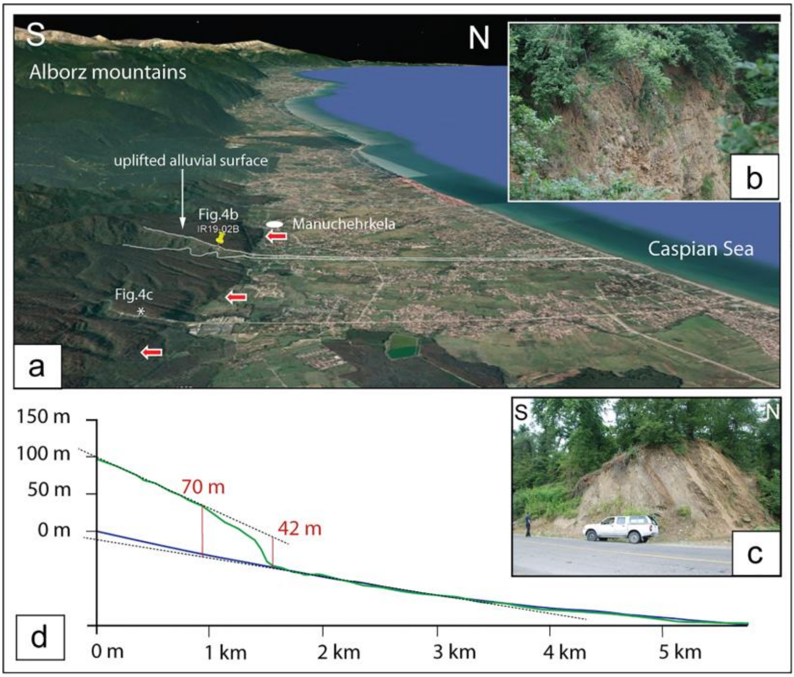

Figure 4: (a) Westwards Google Earth view showing a cumulative fault scarp associated with the Khazar Fault near the village of Manuchehrkola. The white lines indicate the two topographic profiles shown in (d); the yellow arrow points out where sample IR19-2B was collected; (b) Field picture showing the alluvial deposits associated with the uplifted surface; (c) Field view of the ancient tilted deposits in front of the fault-propagation fold; (d): topographic profiles (top of the terrace riser and the river bed). (For interpretation of the references to color in this figure legend, the reader is referred to the web version of this article.)

Table 1: ^{14}C age of sample IR19-2B (see Fig. 4a for sample location). The sample was prepared following the LMC14 protocol (Dumoulin et al., 2017). Measurements were performed at Artemis National Facility: Plateforme Nationale LMC14, CEA Saclay- Bˆat.450- Porte 4E-91191GIF sur YVETTE Cedex; Moreau et al., 2013).

Nature	mgC	Delta C13	pMC*	Age BP	Cal BP
Silt	0.51	–22.4	5.0011 ± 0.044	24050 ± 70	28085 ± 262

* Corrected for splitting.

1-2-3- Evidence of surface ruptures along the Khazar fault

Although the Khazar Fault is mostly hidden, morphological characteristics of a few places suggest that the fault plane locally reaches the surface. One example is near the SE corner of the Caspian Sea, 8 km to the east of Behshahr (Figure 1). Figure 5a shows a 3D view of a fault scarp, affecting a young alluvial surface on which the village of Khalil Shar is built, at the expected location of the Khazar Fault. The height of the scarp is 11.4 to 17.4 m (Figure 5b).

A Malå Geoscience system with 250 MHz shielded antennas was used to collect ground-penetrating radar (GPR) data along a 180 m profile across this scarp (Figure 5c, d). Besides, 75 apparent resistivity data were measured along the same profile. Electrical resistivity tomography (ERT) data were measured with an ABEM SAS 300 system with a dipole–dipole electrode configuration using 19 electrodes. The electrode spacing was set to 10 m (i.e., a =10 m) and data were collected for 6 levels (i.e., n =1:6). The skin effect due to conductive subsurface sediments limited the depth penetration of GPR data to the top 2 m of sediments (e.g. Nabighian, 1991). However, these high-resolution reflectors are visibly deflected near the topographic scarp (red arrow in Figure 5c). Recent tectonic activity can disturb shallow Quaternary deposits, even in such conductive sediments (less than 100Ωm).

Automatic gain control (AGC), and trace averaging (Neal 2004) used for the processing of the GPR data. An average GPR pulse velocity of 0.1 m/nS was used for time-to-depth conversion. The model from 2D inversion of ERT data using the least-square method (Loke, 2015) is presented in Fig. 5d. At the scarp location, the resistivity model shows a very faint lateral variation that could tentatively match the southwards dipping Khazar Fault.

Paleoseimic investigations at Gohar-Tappe archeological site – Outcrop evidence of the Khazar Fault at the Gohar-Tappe archeological site (36º 40′43′′N, 53º 24′01′′E), ~12 km to the west of Behshar (Figure 6), on a ~ 600 m long, ~400 m wide, and ~ 10 m high hill of sand and loess. This isolated, oval shaped hill, 1–1.3 km north of the main break of slope of the Alborz Mountain range, is one of the largest archaeological sites in northern Iran. Between 2000 and 2002, during a reconnaissance survey carried out by the Cultural Heritage Organization mof Mazandaran (MCHO), prehistoric artifacts were discovered, which motivated joint Iranian-German archeological investigations in the following years (Piller and Mahfroozi, 2009). These investigations revealed that the pre-historic site of Gohar-Tappe was a Bronze Age city. The lower layers of the site represent a late fourth-millennium occupation, and settlement continued until around 1500 BCE (Piller and Mahfroozi, 2009). During a visit of the trenches of the archeological site in 2013, we identified faults cutting through the near-surface deposits (Figure 6 to Figure 8). These surface ruptures and the fact that they are located within a relief situated in front of the Alborz Mountain foothills led (Nazari et al., 2021) interpreting the Gohar-Tappe site as a young foreberg structure (seesection 3.1).

In 2014-2018 they ran a subsurface geophysical survey of the site to study the structures at depth. They investigated a 740 m long profile across the hill using the ERT method (Figure 7a). The data were acquired using a dipole–dipole array with an electrode spacing of 20 m. In areas with distinct resistivity contrasts or topographic variations, they used smaller electrode spacing of 10 m and carried out GPR and magnetometric surveys (e.g. Alahverdi Maygooni et al., 2019) (Figure 7b, c). These geophysical methods are sensitive to disparate physical and geometrical properties of the subsurface structures and provide different resolutions and depths of investigation (Gallardo and Meju, 2011; Mohammadi Vizheh et al., 2020).

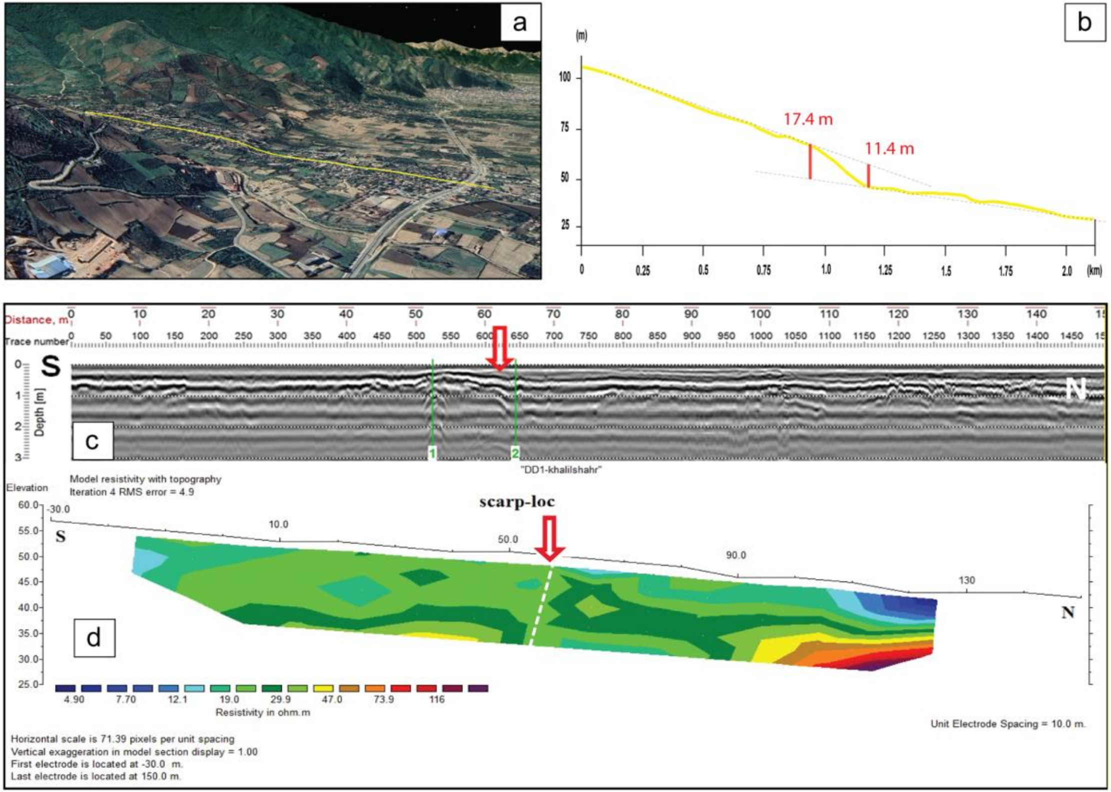
a
b
(m)
17.4 m
11.4 m
(km)
c
Distance, m
Trace number
Depth [m]
S
N
"DD1-khalilshahr"
d
Model resistivity with topography
Iteration 4 RMS error = 4.9
Elevation
scarp-loc
Resistivity in ohm.m
Unit Electrode Spacing = 10.0 m.
Horizontal scale is 71.39 pixels per unit spacing
Vertical exaggeration in model section display = 1.00
First electrode is located at -30.0 m.
Last electrode is located at 150.0 m.

Figure 5: (a) Westwards oblique view of a Google Earth Landsat satellite image (http://www.earth.google.com) showing a fault scarp associated with the Khazar Faultin the region of Khalil Shar. (b) Topographic profile across the fault scarp shown in a. (c) Processed GPR profile acquired using a Malå Geoscience system and antennas with center frequencies of 250 MHz, average GPR pulse velocity of 0.1 m/nS (we used standard processing steps such as band-pass filtering, background removal, normal moveout correction, AGC gain and trace averaging (Neal, 2004); the red arrow points out the scarp observed in the landscape. (d) Corresponding resistivity profile with 2D data inversion using the least-square (Loke, 2015) method. (For interpretation of the references to color in this figure legend, the reader is referred to the web version of this article.)

The same instruments and techniques as in Khalil Shar site were used for ERT and GPR data acquisition, as well as data processing and ERT data inversion. In total, 349 apparent resistivity data were measured along the profile. The model from 2D inversion of ERT data shows that resistivity values of the subsurface structures are from 1 to 70 Ωm, due to the thick Quaternary cover of wet, fine-grained sediments (e.g. clay to silt; see Figure 6).

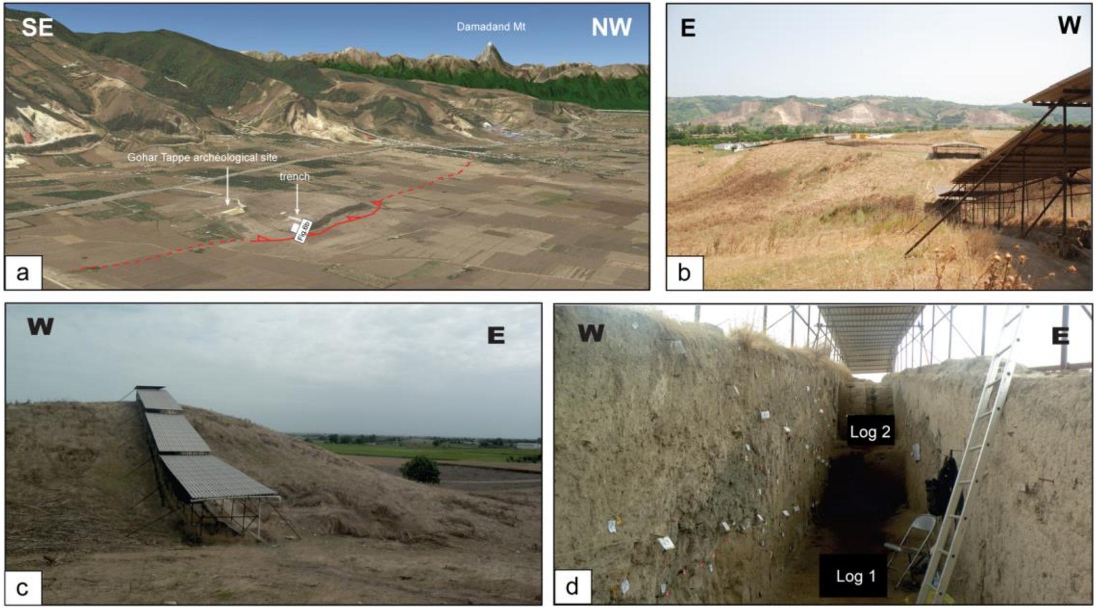

Figure 6: (a) South-westwards Google Earth view of the foothills of the Alborz at the archeological site of Gohar-Tappe; (b) Field picture showing the site. The metallic roof to the right covers the archeological trench; (c) Field picture showing the trench from the south; (d) A view inside the trench.

The resistivity profile shows distinct contrasts that match with the main topographic scarps, notably within the northern part of the hill (240–300 m, Figure 6)) where several steep discontinuities are observed, and within the southern part of the hill (at 50 m, Figure 6) where there is major discontinuity. These resistivity discontinuities interpret as secondary steep normal faults above the frontal part of the foreberg and back thrust-fault at the rear of the foreberg, respectively, while the main thrust fault remains hidden (see Bayasgalan et al., 1999 Figure 4 & Figure 3c). The magnetic records (Figure 7b), also show a clear variation in the signal matching with the resistivity model within the topographic scarp at the rear of the hill. The two GPR sections show several discontinuities (e.g. at 270 m and 280 m, Figure 6) in the stratigraphic layers in the northern part of the hill. The observed undulations of GPR reflectors between 400 and 460 m reflect variations in the corresponding resistivity model (Figure 7a) and can be interpreted as a highly fractured area (Figure 7c). The various sub-surface geophysical signals are coherent.

A detailed stratigraphic study also carried out in Gohar Tappe archaeological trench, located in its northern part (Figure 8), to look for evidence of deformations or fault planes. The trench shows a sequence of well-stratified silty-clayey units interpreted as a succession of flood plain and/or lagoon episodes. The units dip ~ 15◦ to the north and areaffected by several steep normal faults (F) and fractures (f), associated with a few reverse faults (Figure 8b). These structures are consistent with the features observed within the sub-surface geophysical survey (see Figure 7a, c), and interpreted as steep normal faults tilted with the stratigraphic units within the northern limb of the foreberg.

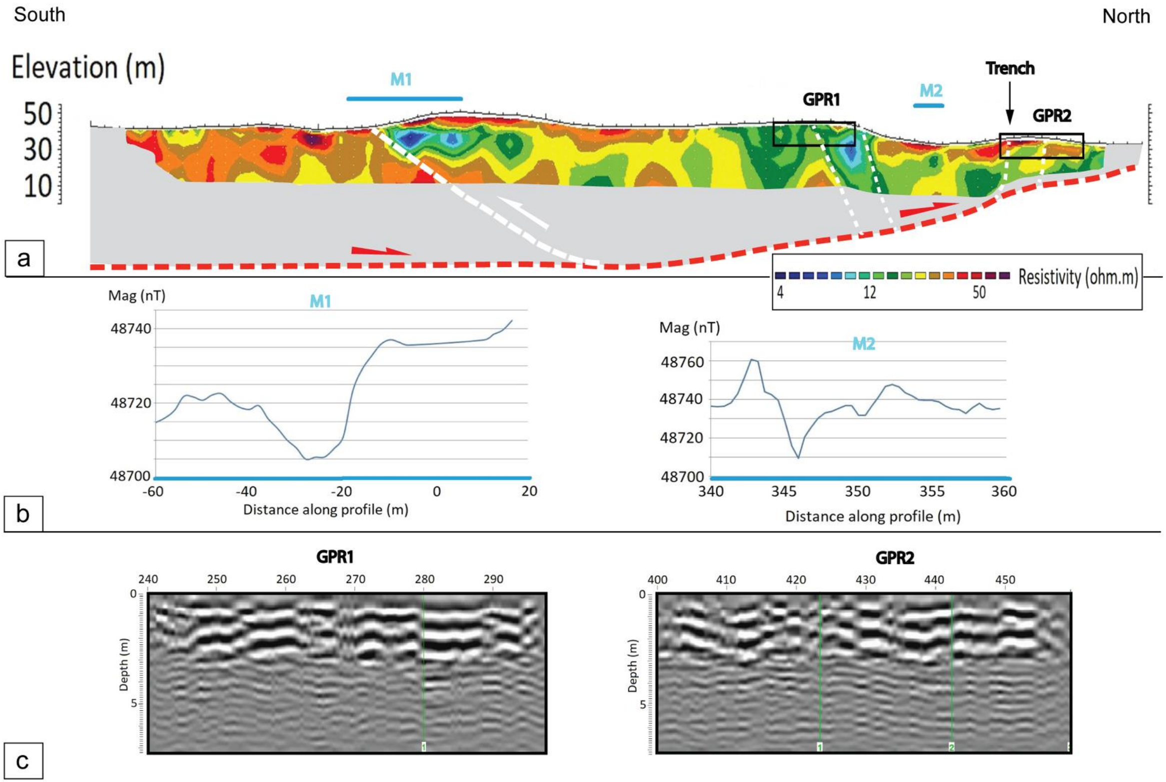

South
North
Elevation (m)
50
30
10
M1
M2
GPR1
Trench
GPR2
a
Resistivity (ohm.m)
4
12
50
Mag (nT)
M1
48740
48720
48700
-60
-40
-20
0
20
Distance along profile (m)
Mag (nT)
M2
48760
48740
48720
48700
340
345
350
355
360
Distance along profile (m)
b
GPR1
240
250
260
270
280
290
Depth (m)
GPR2
400
410
420
430
440
450
c

Figure 7: Joint interpretation of geophysical datasets along Gohar-Tappe site. (a) Resistivity model from 2D inversion of DC resistivity data (dashed white lines for interpreted faults, dashed red line corresponds to the supposed flat thrust fault beneath the foreberg). (b) Magnetic profiles; (c) Processed GPR sections using 100 MHz shielded antennas. (For interpretation of the references to color in this figure legend, the reader is referred to the web version of this article.)

Detailed logging of the stratigraphic units revealed many fragments of pottery and other artifacts associated with the human occupation, among which pieces of charcoal were collected for radiocarbon dating. They yielded calibrated ages between 5500 and 3800 BP, which are consistent with the archeological study of the Gohar-Tappe site (Piller and Mahfroozoi, 2009). Four samples (C77, C72, C57, and C37) in Log and one (C3) in Log 2 are not in stratigraphic order. They probably correspond to reworked detrital charcoal from older units. One sample (C13) is much younger than other ages and may reflect contamination an analytic error. Those six samples have been discarded from the paleoseismic analysis.

To decipher the different paleoseismic events, Nazari et al., (2021) used fault-terminations sealed by overlaying units as well as the variations in offset along faults between one stratigraphic unit and the subsequent one (e.g., McCalpin, 2009). A first event is identified within faults and fractures f5, F5′, f7, F10, f10′ in Log1, and F12, F13 in Log 2, which all affect the youngest dated units and 5 in Log1, and Log 2, respectively. These faults and fractures are younger than 3976 ± 152 cal BP, which is the age obtained for sample C20 collected in unit 17 (Table 2). Note, however, that the faults along which the base of unit 17 (Log 1) and unit 5 (Log 2) are offset (F10 in Log 1, F12 and F13 in Log 2) may correspond to different events that also affected the ground surface units 19 (Log1) and 7 (Log2), and that there are no younger deposits to establish precisely Their temporal distribution.

The second event is well characterized by several fault termination criteria observed along faults and fractures F1, f4, f6, f8, f8, F9, and F11 in Log1, which are overlain by units 17–16 in Log 1. Radiocarbon ages show that this event occurred between 3824 cal BP C71).

A third event can be interpreted along fault F10, where the base of unit 3 shows a much larger offset than the bases of overlaying units 6 and 10. Moreover, along this same fault, unit 3 was eroded by the overlaying unit 4a, which corresponds to tilted stratified silts and clays, rich in clasts (20%), with a clear upward sorting. We interpreted these deposits as a post-event unit, in which localized deposition was controlled by F10 free face. After radiocarbon ages, this third event occurred between 4844 cal BP (i.e. 5021–177 yrs, sample C7) and 5214 cal BP (i.e. 5057 + 157 yrs, sample C47). Therefore, at least 3 surface-rupturing events occurred in the past 5300 yrs (5198 cal BP +the past 70 yrs between 1950 and 2020), with 2 events between 3976 ±152 and 5057 +157 cal BP. A time interval of 1000 ±400 yrs separate these two last events. Considering the upper bound of this interval (i.e., 1400 yrs) as a maximum mean recurrence interval for surface rupturing events along the Khazar Fault, suggests that at least 2 more events occurred during the past 5300 yrs.

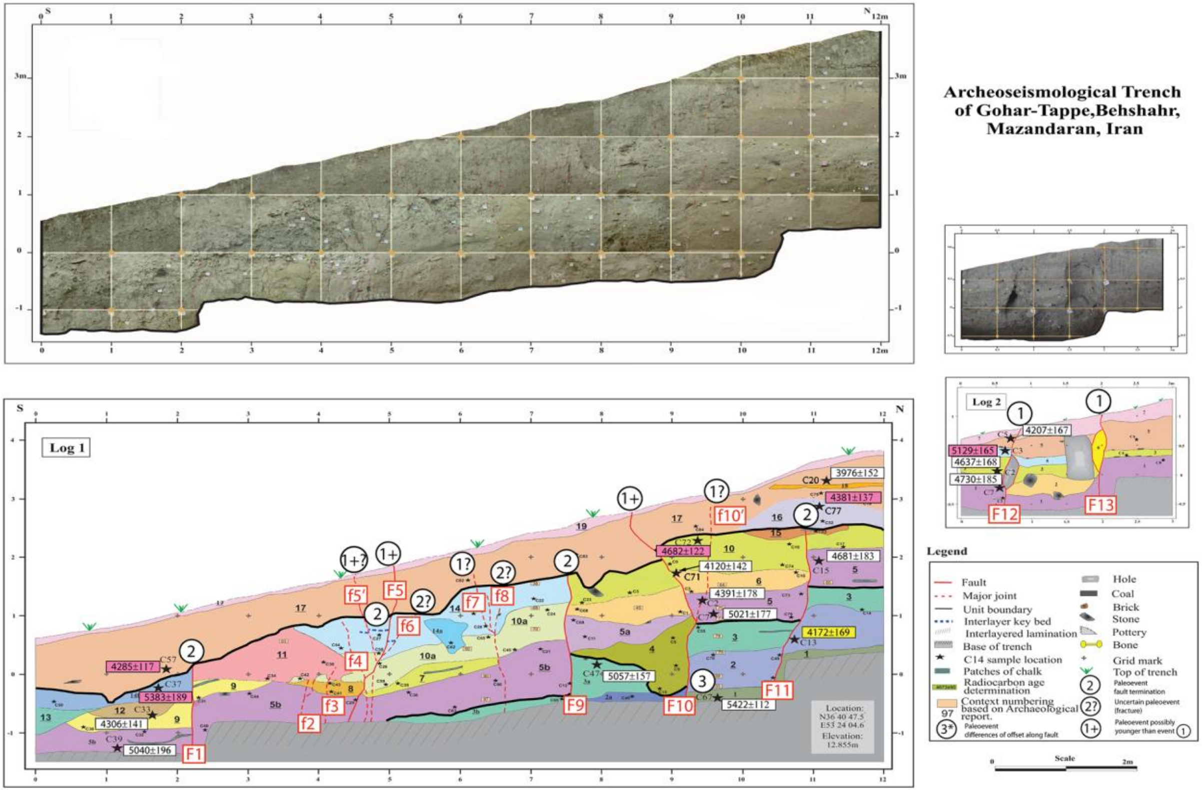
Archeoseismological Trench
of Gohar-Tappe,Behshahr,
Mazandaran, Iran
Log 1
Log 2
Location:
N36 40 47.5
E53 24 04.6
Elevation:
12.855m
Legend
Fault
Major joint
Unit boundary
Interlayer key bed
Interlayered lamination
Base of trench
C14 sample location
Patches of chalk
Radiocarbon age determination
Context numbering based on Archaeological report.
Paleoevent differences of offset along fault
Hole
Coal
Brick
Stone
Pottery
Bone
Grid mark
Top of trench
Paleoevent fault termination
Uncertain paleoevent (fracture)
Paleoevent possibly younger than event 1
Scale
0
2m

Figure 8: Photomosaic (a) and interpretative log (b) of the western wall of the re-occupied archeological trench in Gohar-Tappe prehistoric site. Event Horizons shown by thick black line in Log1. Logs 1 and 2 are separated by ≤2 m. Colors allow following the correspondence of the different stratigraphic units between the 2 logs. Description of units in Log1: U1: Light brown silts and clays, ≤5% clast, a few pieces of pottery; moderate consolidated, non-stratified (flood plain or lagoon deposits). U2: Grayish brown silts and clays, ≤3% clast (1–3 mm), porous texture, sporadic chunks of charcoal, a few pieces of red to brick color potteries mostly in the lower part (less than unit1) (flood plain/lagoon deposits). U2a: similar to the upper part of U2. U3: Light brown, ~1% clast (1–3 mm), a few pieces of pottery less than in U2, sporadic chunks of charcoal, brick color patches (2 mm, rarely up to 2 cm), in some part thin layers of carbonaceous, moderate consolidated, stratified (flood plain/lagoon deposits). U4: Multi-colored silts and clays, alternation of white, gray, and brown, increase of silts upward, 20% clast (1–5 mm, rarely 3–7 cm of chert), clasts often have brick color, pieces of pottery (often 12 cm), numerous charcoals, loose to medium compaction, more consolidated in the upper part, bits of bone, tilted layers upward, similar to unit 3. U5: Grayish brown silts and clays, a few clasts (1–3 mm), pieces of pottery, stone tools, brick color patches (1 mm-10 cm) more than in units 1–4, consolidated, in some parts thin layers of carbonate, sporadic charcoals and chunks of bones (animal?), chalk (thickness 3–7 cm) in the lower part. U6: Gray lens of silts and clays, (10–15% clasts (2 mm-1 cm, rarely 3 cm), non-stratified, angular to subangular, abundant pieces of charcoal, pieces of pottery bones (animal?) and teeth (human?), brick color patches (2 mm-3 cm), a piece of brick 5 cm6cm. U7: Gray lens of silts, 10–15% clast (2–5 mm), sorted, patches brick color (2–3 mm, up to 1 cm), pieces of pottery in base (7–1 0 cm), interlayers of chalk (thickness 1 cm), charcoals and chunks of bones, non-stratified, similar to unit 6. U8: Grayish buff, alternating of thin layers of silts and carbonaceous (3–4 cm), stratified, less 5% clast (1–3 mm up to 5 mm), pieces of pottery (1–8 cm), patches brick color (5 mm-5 cm), loose to moderate hardness. U9: Grey silts and clays, a few clasts (1–3 mm), pieces of pottery (rarely 8 cm), patches brick color (2 mm-30 cm), the thick brick color 4 cm in the top, charcoals, thin

layer of charcoal at the base in the northern part, sporadic fractures, similar to units 6,7 and 8. U10: Light brown silts and clays, 5–10% clast (1–5 mm, rarely 1–2 cm), sub-rounded, abundant brick color patches (2–4 mm, up to 1-3cmm), pieces of pottery (1–7 cm), pieces of bones, sporadic chunks of charcoal, medium compaction, non-stratified (flood plain/lagoon deposits). U11: Non-situ, gray silts, and ashes (peat?), without clast, sporadic charcoals increasing at the base of the unit, brick color patches (6–12 cm), loose (flood plain deposits). U12: Gray lens, alternating layers of silts and carbonates (ashes?), without clast, patches brick color (0.5–3 cm), pieces of pottery (1–2 cm up to 10–12 cm), a few chunks of charcoal, loose, carbonaceous in the upper and lower part, silty in the central part, moderate compaction, like in unit 11. U13: Cream to buff silts and clays, 5–10% clast (2 mm-lcm), a few patches brick color (0.5–1 cm), pieces of pottery (1–3 cm, rarely 7 cm), subrounded, weakly stratified, alluvium deposits? U14: Separate in unit 10, brick color, abundant patches brick (2 mm-lcm), carbonaceous in northern part at the top of the unit. U15: Cream to brown silts and clays, 3–5% clast (2–5 mm) decreases to the north, pieces of pottery, patches brick color (2–3 cm), the thin layer of brick in the northern part (thickness 5 cm), pieces of bones, moderate compaction, non-stratified (flood plain/ lagoon deposits). U15a: similar but looser than U14. U15b: Cream to brick, 2–3% clast (2–3 mm up to 2 cm), pieces of pottery, charcoal, consolidated (in the southern part) which decrease in the northern part, weakly stratified (flood plain/ lagoon deposits). U16: Grey to buff, 5% clast (2 mm-l cm, rarely 3–5 cm), a few pieces of pottery, patches brick (0.5–2 cm), a few charcoals, loose compaction, weakly laminated, root print in some part (flood plain/ lagoon deposits). U17: Layers of carbonates and silts, without clast, loose, roots residual, non-stratified. U18: thin carbonate layer. U19: cream to brown, 1% clasts (2–3 mm), a few pieces of pottery, loose, non-stratified, ground surface with residual of roots and erosional channel. Log 2: U1: Light brown silts and clays, ≤3% clast (2–5 mm rarely to 2 cm), pieces of pottery in some part, contain thin layers of chalk, charcoals, compact, weakly stratified (flood plain deposits). U2: Cream silty layer, non-stratified, contain pottery crumbs, 2 pieces of stone (15–25 cm), similar to handmade soil. U3: Light brown to cream silts and clays, none stratified, consolidated, ≤3% clast, pieces of pottery, a charcoal layer at the base of unit mostly in the northern part, a thin layer of chalk in the lower part, root print in the southern part. U4: Light creamy silts, non-clear stratified, 2–5% clast (2 mm-5 mm, rarely 1.5–2 cm), pieces of color brick in some part (0.5–1 cm, rarely 2–4 cm), this unit is only seen in this part of the trench (handmade?), more consolidated than unit 3. U5: Cream to light brown silts and clays, no-clear stratigraphy, contains pieces of limestone (0.5–5 cm) at the base, contain very little clast (2–3 mm, rarely to 4 cm), pieces of color brick in some parts (0.5–2 cm), some pieces of pottery (rarely 10 cm), more compact at the lower part (flood plain deposits). U6: A mixed material of units 3, 4, and 5. U7: Light brown silts and clays, non-stratified, 1% clast (1 mm- 2 mm rarely 1–2 cm), loose deposits, contain caliche, pieces of pottery (1–6 cm), contain root prints. (For interpretation of the references to color in this figure legend, the reader is referred to the web version of the article by Nazari et.al, 2021.

Table 2: ^{14}C ages (^{14}C laboratory, ETH University), Gohar-Tappe prehistoric site, see Figure 8 for samples location (Nazari et al., 2021)

C14 dating (Gohar-Tappe-Log1)																		
ETH nr.	sample label	^{14}C counts	^{12}C (µA)	$^{14}C/^{12}C$ (10^{-12})	+- (%)	$^{13}C/^{12}C$ (%)	sigma(%)	$F^{14}C$	+- (%)	sig (%)	age (y)	+-(y)	$\delta^{13}C$ (‰)	weight (µg)	$^{13}C(H)$ (nA)	Calendar age (2-σ range)	Calendar age (2-σ range)	Calendric Age CalBP
65986.1.1	GT-C57-2014	12,322	6.9	0.6223	0.90	1.0393	0.07	0.6177	1.06	0.69	3,869	85	-23.3	null	0.04			4285 ± 117
65987.1.1	GT-C77-2014	9,107	6.9	0.6175	1.05	1.0396	0.08	0.6125	1.19	0.77	3,938	96	-23.0	null	0.06			4381 ± 137
65988.1.1	GT-C71-2014	8,832	5.9	0.6236	1.06	1.0320	0.10	0.6277	1.21	1.04	3,741	97	-30.0	null	0.04			4120 ± 142
65989.1.1	GT-C33-2014	7,556	5.9	0.6181	1.15	1.0368	0.09	0.6165	1.29	1.07	3,886	103	-25.5	null	0.03			4306 ± 141
65990.1.1	GT-C13-2014	4,796	6.1	0.6042	1.44	1.0180	0.09	0.6248	1.56	1.57	3,778	125	-43.2	null	0.06			4172 ± 169
66124.1.1	GT-C37-2014	5,370	4.1	0.5328	1.36	0.9944	0.02	0.5565	1.76	1.41	4,708	141	-36.7	null	0.03			5383 ± 189
66125.1.1	GT-C20--2014	11,000	6.3	0.6150	0.95	1.0004	0.04	0.6357	1.37	0.88	3,639	110	-30.1	null	0.05			3976 ± 152
66126.1.1	GT-C7-2014	10,466	6.5	0.5633	0.98	1.0003	0.03	0.5814	1.43	1.07	4,356	115	-30.1	null	0.06			5021 ± 177
66129.1.1	GT-C2-2014	8,854	6.1	0.5773	1.06	0.9872	0.06	0.6124	1.48	0.80	3,940	119	-43.0	null	0.03			4391 ± 178
67971.1.1	GT-C39-2014	5,336	6.0					0.5795	0.0103		4,383	142	-26.1	null		3,497	2,626	5040 ± 196
67976.1.1	GT-C15-2014	4,759	5.0					0.5954	0.0109		4,165	147	-29.5	null		3,308	2,295	4681 ± 183
	GT-C67 2014	11,641	6.8	0.6335	0.93	1.0886	0.03	0.5589	1.12	0.92	4,673	90	-22.7	null	0.23			5422 ± 112
	GT-C47 2014	10,777	6.4	0.6553	0.96	1.0887	0.03	0.5787	1.15	0.82	4,394	92	-22.6	null	0.28			5057 ± 157
	GT-C72 2014	10,420	6.1	0.6783	0.98	1.0920	0.03	0.5959	1.16	1.06	4,159	93	-19.6	null	0.23			4682 ± 122
C14 dating (Gohar-Tappe-Log2)																		
67974.1.1	GT2-C2-2014	6,619	5.8					0.5984	0.0098		4,124	132	-27.7	null		3,017	2,300	4637 ± 168
67975.1.1	GT2-C7-2014	5,510	5.4					0.5931	0.0103		4,196	140	-28.2	null		3,326	2,351	4730 ± 185
66130.1.1	GT2-C3-2014	9,754	6.5	0.5514	1.01	0.9973	0.03	0.5722	1.47	0.92	4,485	118	-33.0	null	0.08			5129 ± 165
66128.1.1	GT2-C5-2014	10,548	6.3	0.5954	0.97	0.9947	0.05	0.6223	1.40	1.06	3,811	113	-35.6	null	0.03			4207 ± 167

1-3- Discussion

Although there is a clear morphotectonic features associated with Late Quaternary activity of the Khazar Fault, few possible candidates found for the surface outcrop of the thrust fault, which makes a precise determination of its position and paleoseismological analysis difficult.

In the middle segment of the fault, near Chamestan city, the fault-bend fold uplifting an alluvial terrace allowed estimating a minimum vertical slip rate of 2.0 ±0.5 mm yr, which is consistent with the uplift rate of 1.9–2.8 mm/yr deduced from the incision rate in the Garmrud valley, 50 km to the east from the study site (Antoine et al., 2006). This yields a minimum Late Quaternary average slip rate along the Khazar Fault of 3.6 mm/yr, in consistency with the rate of 4–6 ± 2 mm/yr estimated from a GPS-derived fault-block model (Djamour et al., 2010).

The fact that there are morphological scarps along the Khazar Fault zone shows its ability to produce surface ruptures. This observation associated with the fact that the fault can generate earthquake as deep as 22 km (Tatar et al., 2007) involves that the Khazar Fault is likely capable to generate large (Mw7) to very large (Mw8) events, which is consistent with the estimate of the magnitudes that can be made from the Khazar Fault segmentation deduced from the direction changes of the slope break at the northern foothills of the Alborz. (see section 3.1).

The geophysical and paleoseismological analysis at the archeological site of Gohar-Tappe leads to propose that the site upon a young foreberg structure affecting Holocene deposits. Paleoseismological vestigations suggest that at least five events occurred in the past 5300 yrs, considering a mean maximum interval of 1400 yrs. This recurrence interval and the minimum slip rate along the fault yields a minimum seismic slip along the fault during large surface-rupturing events comprised between 2 and 5 m, which is consistent with the range Mw7-8 Moment magnitudes estimated from the Khazar Fault dimensions.

It is worth noting that the sedimentary units in Gohar-Tappe correspond mainly to flood or lagoon deposits, with no deposits younger than ~ 3800 yrs. This is consistent with the interpretation that this site corresponds to a recent foreberg structure that raises above the base level e. the Caspian Sea level) ~ 3900 years ago. The structure cumulates nowadays ~ 10 m of uplift, which suggests that several events have occurred since then. One of these events could correspond to the 1809

BCE (=3759 cal BP) event, which affected the Amol region (Berberian,1996). This historical event could correspond to event 1 identified in the trench, which occurred after the deposition of unit 17 (dated at 3976 152 yr).

Unfortunately, we have no age constraints to bracket the age of event 1. However, we tentatively propose that it occurred not long after the deposition of unit 17, given that no another sedimentary unit covers it. It is also worth noting that archeologists did not find evidence of human settlement younger than ~ 3500 cal BP on the site. This attests to the abandonment of the prehistoric site, which, like many other pre-historic sites in eastern Alborz, can be related to a destructive earthquake or a sequence of strong earthquakes.

1-4- Conclusion

The analysis of the Khazar Fault in northern Alborz has revealed new insights into its activity.

Generally classified as a hidden thrust fault associated with fault-propagation, fault-bend folds, and foreberg structures, the Khazar Fault also appears to be active within the mountain range. Its southward dip and potential to generate deep earthquakes of 20–30 km pose significant seismic hazards to densely populated areas. The steep slopes in Alborz mean that a strong earthquake would likely trigger numerous landslides and rock avalanches, damaging roadways and increasing the risk of building destruction. Furthermore, recent geological surveys have emphasized the complex interactions between the Khazar Fault and adjacent tectonic structures. These interactions may play a critical role in the fault's behavior and its earthquake potential. Field studies have uncovered fault traces and sedimentary deposits that indicate prior seismic events, adding to the historical context of the region's seismicity. Monitoring stations installed along the range have started to record microseismic events, suggesting that even minor movements along the fault may be precursors to larger ruptures. The analysis of these low-magnitude earthquakes could provide vital data for understanding the stress accumulation along the fault plane. The implications for local communities are profound.

Improved risk assessment and urban planning strategies are necessary to mitigate the potential impacts of a major seismic event. Enhanced early warning systems, coupled with public education on earthquake preparedness, could save lives and reduce property damage. In addition, interdisciplinary collaboration between seismologists, geologists, and urban planners is essential to formulate comprehensive hazard mitigation plans. As research continues to uncover the dynamics of the Khazar Fault, ongoing efforts to better understand its behavior will be crucial to safeguarding those residing in this seismically active region. Such initiatives not only enhance the resilience of infrastructure but also empower communities to respond effectively in the face of natural disasters.

PART II Geophysical Investigation

2-1- Introduction

Khalil Shahr and Gohar Tappe were selected for geophysical studies. In Khalil Shahr, two GPR profiles were surveyed: profile 1 at 150 meters and profile 2 at 37 meters, using 100 and 250 MHz non-covering antennas. Resistivity measurements were taken with a dipole-dipole arrangement at 76 points, spaced 10 meters apart on profile 1. In Gohar Tappe, studies expanded to include cesium magnetometry, conducted across two rectangular grids and four linear profiles: grid 1 covering approximately 2,500 square meters and grid 2 about 15,000 square meters. Additionally, magnetic susceptibility measurements were performed at various depths to complement the cesium magnetometry data. These measurements focused on understanding the subsurface lithology and identifying potential buried features. In total, 120 susceptibility readings were obtained from Gohar Tappe, with a sampling interval of 5 meters along the linear profiles (Table 3).

To further enhance the geophysical understanding of both sites, a series of seismic refraction surveys were conducted at strategic locations within the surveyed areas. The seismic surveys utilized a spread of geophones arranged in a linear array to ascertain the velocity of seismic waves through differing material layers. This data aimed to elucidate the structural characteristics and stratigraphy of the subsurface environment, which, combined with the resistivity and magnetic data, would provide a holistic view of the geological framework.

Moreover, the integration of geological mapping and soil sampling in the fieldwork added a vital context to the geophysical findings. Soil samples from both Khalil Shahr and Gohar Tappe were collected at depths of 0.5 meters and 1 meter to analyze their chemical properties and correlate them with the geophysical anomalies identified.

This multi-faceted approach allowed for a comprehensive geophysical study that not only embraced traditional methods but also utilized modern techniques to better understand the geological history and potential resource locations of the surveyed regions. Ultimately, the findings from these studies are expected to contribute to a clearer interpretation of subsurface conditions, aiding in future exploration projects and environmental assessments within these areas.

Table 3: Characteristics of the magnetic surveyed profiles in Gohar Tappe region

Profile name	**Start of profile**	**End of profile**	**Azimuth**
4500	714500, 4061600	714500, 4062070	˚0
4530	714530, 4062110	714530, 4062245	˚0
4630	714630, 4062110	714630, 4062310	˚0
1	714544, 4061533	714517, 4061890	˚0

In this area, GPR survey was performed on a rectangular grid and a linear profile. A grid survey on grid number 1 (grid1) including 50 to 20 profiles that are located at a distance of 10 meters from each other and a linear survey on 5 pieces of profile number 1 with different lengths and using two 100 and 250 MHz antennas were made uncoated.

2-2- Combining the results of geophysical surveys in Gohar Tappe area

In order to combine the results of geophysical surveys in the Gohar Tappe region, in the places where the results of two or three surveying methods show the same anomaly, the results are brought together for comparison and review. In the following, some of these areas are mentioned and the results obtained from them are presented. Geographical location of Gohar Tappe and Khalil Shahr are shown in Figure 9 & Figure 10, and location of surveyed points is given in Figure 11.

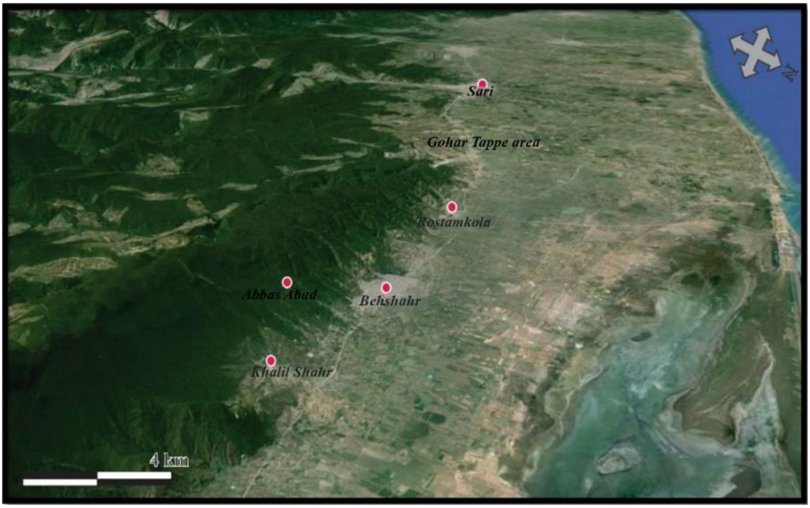

Figure 9: Aerial image of Khalil Shahr and Gohar Tappe areas

Figure 10: Access roads to Khalil Shahr and Gohar Tappe areas

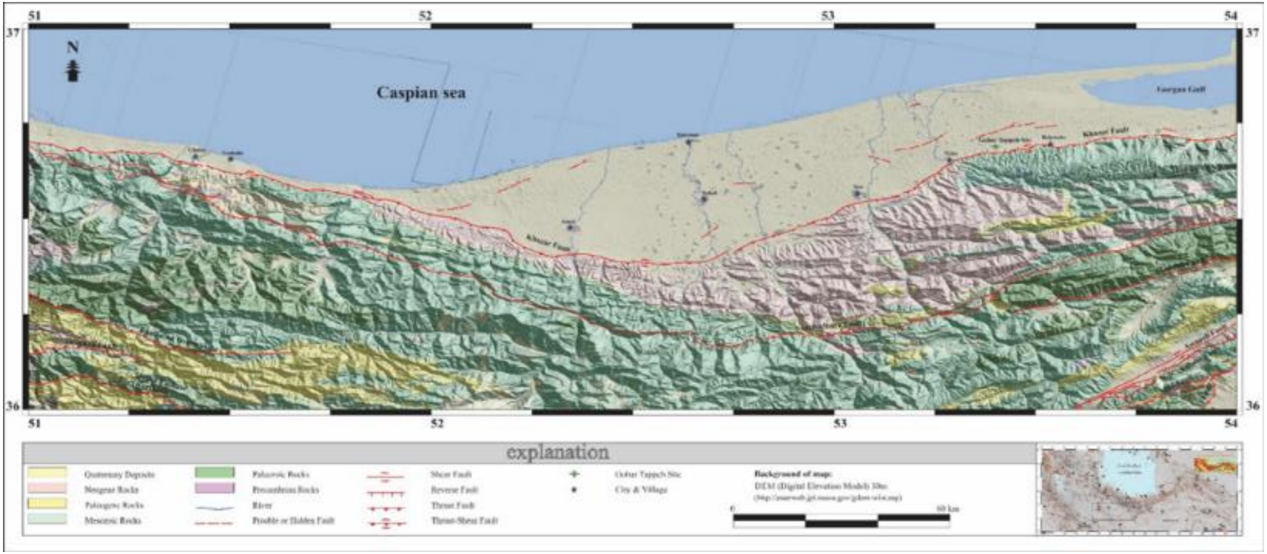

Figure 11: Location map of profiles and surveying networks in Gohar Tappe area

2-2-1- Compilation of specific resistivity model and total magnetic field intensity diagram of profile number 1

Figure 12 shows the Anomaly location profile number 1. In Figure 13, the specific resistivity model with 10 meters electrode distance is shown along with the graph obtained from the magnetometric survey on profile number 1 from station 60-160. The results of both methods, and resulted anomaly between the stations -40 and 0 can be seen in Figure 13. This anomaly has been repeated in the apparent specific resistivity surveying with an electrode distance of 20 meters (Figure 14).

Figure 12: Anomaly location between two stations -40 to 0 from profile number 1

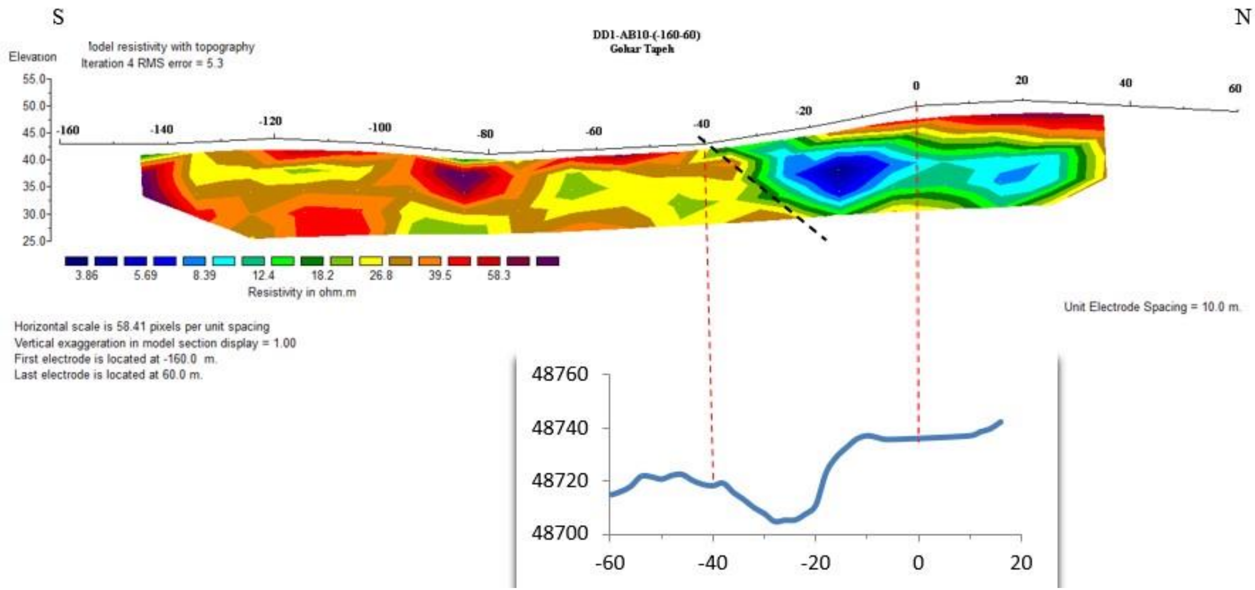

Figure 13: Specific resistivity model with 10m electrode distance along with magnetic diagram on profile number 1

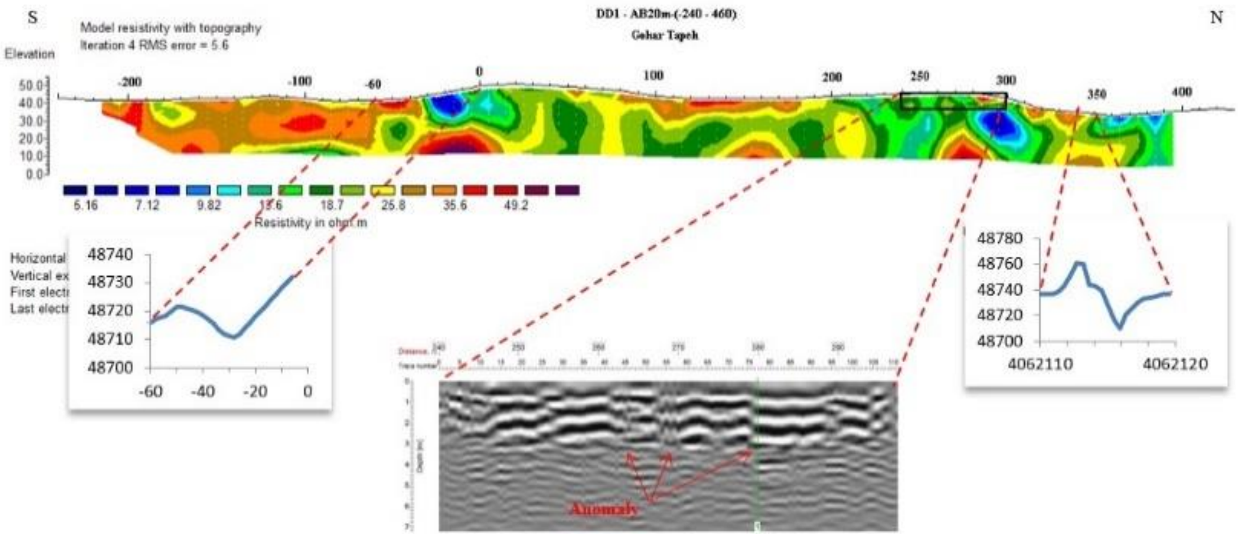

Figure 14: Model of specific resistivity and anomalies of profile number 1

2-2-2- Compilation of results of all three methods on profile number 1

In Figure *14*, the specific resistivity model with an electrode distance of 20 meters, together with the graph obtained from the magnetometric survey from station -60 to 0, as well as the GPR result from station 240 to 300 on profile number 1 and the graph obtained from the magnetometric survey from stations 340 to 350, it is shown on profile 4530. In the results obtained from all three methods, anomalies can be seen between stations 60 to 0 and 240 to 300, as well as stations 340 to 350.

2-2-3- Compilation of results on grid number 2

The anomalies that are related to the three linear anomalies (F2, F3 and F4) from the total magnetic field intensity map of grid number 2 shown in Figure 15. In this figure, the anomalies of two specific resistivity sections related to profile number 1 and the magnetic anomaly of profile number 1 and two anomalies in the magnetic profile of number 4530 are presented. The white lines that can be seen in the total magnetic field intensity map of Network No. 2 are related to the borders between the agricultural lands, and probably are made by the farmers.

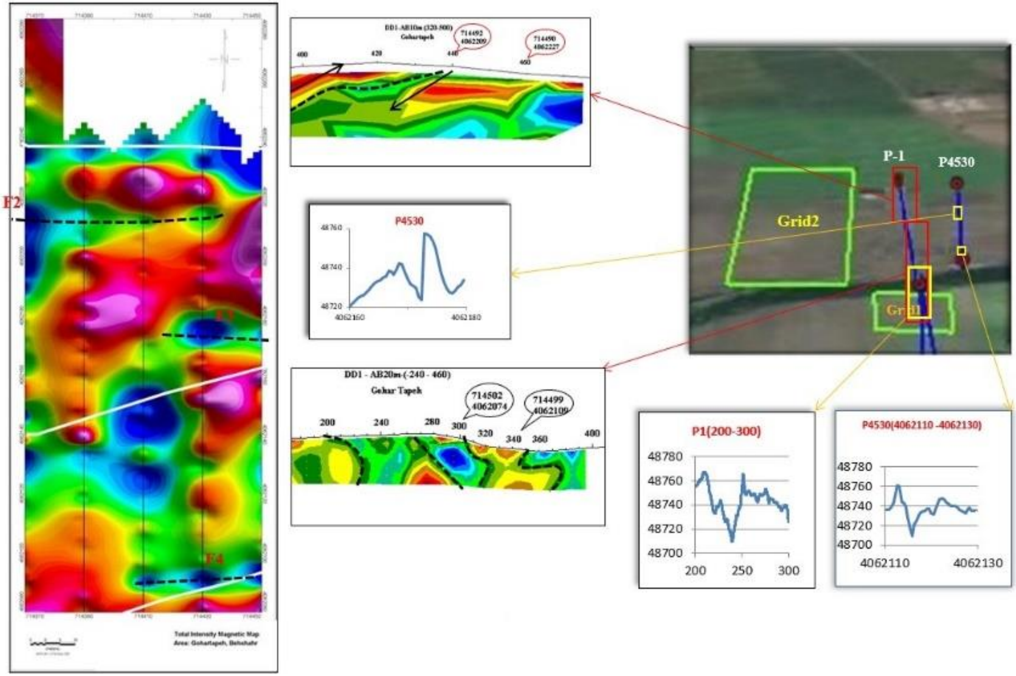

Figure 15: Combining the results with the total magnetic field intensity map of grid 2

2-2-4- Compilation of results on grid number 1

In Figure 16 toFigure *18*, the combination of three-dimensional GPR maps and the map of the total magnetic field intensity of network No. 1 and the matching of anomalies in both maps are presented.

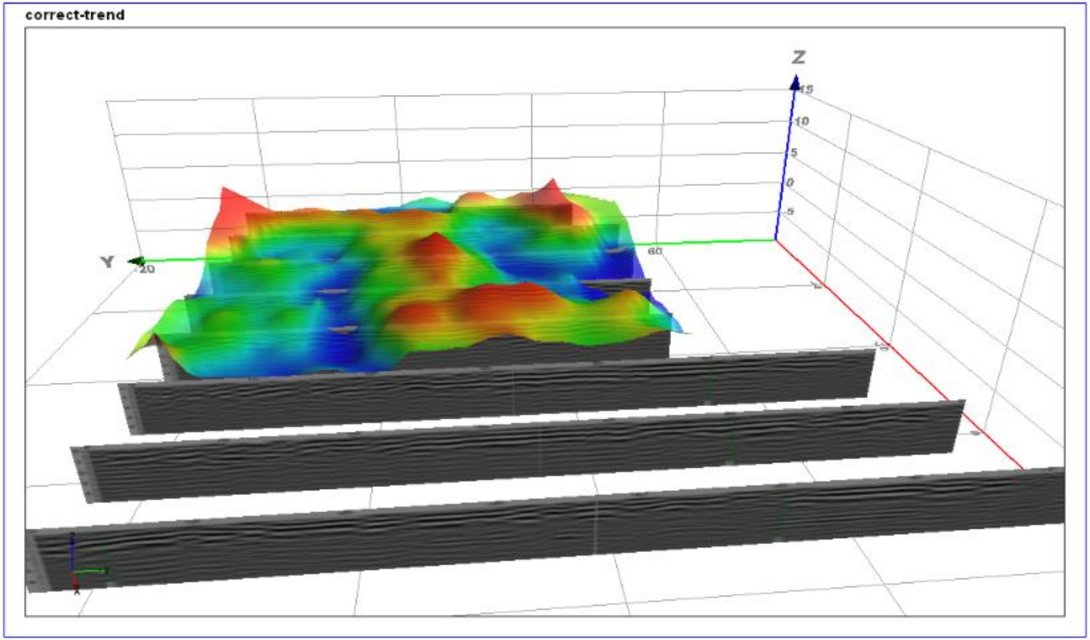

Figure 16: A view of the depth sections of the GPR profiles along with the map of the total intensity of the magnetic field of grid 1

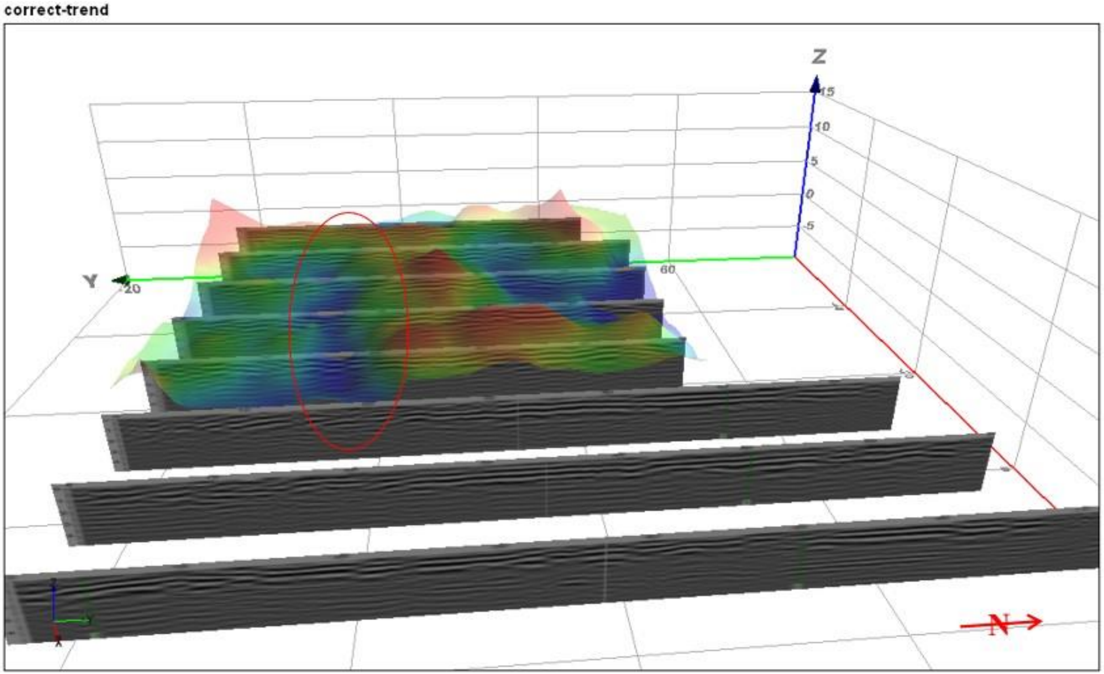

Figure 17: A view of the location of the anomaly on grid 1

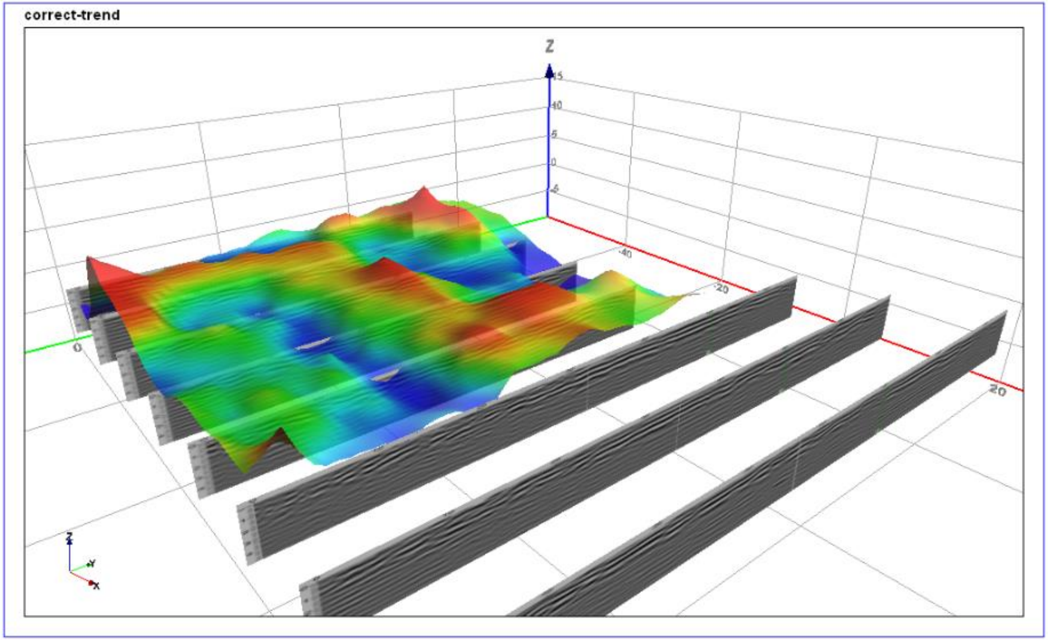

Figure 18: Another view of the depth sections of the GPR profiles along with the map of the total intensity of the magnetic field of grid 1

2-3- Conclusion and Recommendations

Geophysical surveys in the Gohar Tappe area utilized electrical resistivity, GPR, and cesium magnetometry methods. Initial surveys employed electrical resistivity with 20-meter electrode intervals across the historical hill. Subsequent measurements involved shorter electrode distances and specific cesium magnetometry, with GPR applied to some anomalous areas. In the Khalil-Shahr region, resistivity and GPR results along the main east-west street showed little distinction, but identified anomalies may relate to tectonic activities. The geophysical anomalies recognized in Gohar Tappe and Khalil Shahr include:

1. Profile 1 anomalies between stations -60 to 0, 260 to 280, and 340 to 350 (Figure 14).

2. Anomalies F2, F3, and F4 from the magnetic survey in Grid No. 2, corresponding to the pseudo-sections in Profile No. 1 and magnetic diagram 4530 (Figure 15).

3. An anomaly from the magnetic survey in Grid No. 1 that aligns with the GPR anomaly on the same grid (Figure 16).

4. In Khalil Shahr, the resistivity at station 60 of Profile 1 coincides with the GPR anomaly, indicating the scarp's location (Figure 19 & Figure 20).

These anomalies warrant further investigation, particularly in terms of their geological significance and potential implications for understanding the regional tectonic framework. In Gohar Tappe, the presence of electrical resistivity anomalies correlated with distinct features observed in the GPR profiles suggests the possibility of buried structures or stratigraphic variations that merit deeper exploration. In addition, the presence of the identified anomalies within the magnetic survey, especially those linked to F2, F3, and F4, indicates potential zones of weakness or alteration in the subsurface materials that could have implications for both structural geology and archaeological interests. The intersection of these anomalies with known geological features enhances their relevance in a broader geomorphological context.

Further studies utilizing high-resolution GPR and targeted resistivity measurements could provide deeper insights into the subsurface conditions, revealing more about the material composition and its spatial distribution. This could facilitate improved understanding of historical land use and how past tectonic activities might have shaped the current landscape.

Moreover, while the resistivity and GPR results from the Khalil-Shahr region showed subtle differences, the identified anomalies along the main street present valuable data points for assessing urban planning and infrastructure development in areas at risk of geological instability. The correlation between resistivity at station 60 and the GPR anomaly not only underscores the need for integrated geophysical methods but also points to the significance of interdisciplinary approaches in interpreting geophysical data.

In sum, the geophysical survey results from both Gohar Tappe and Khalil Shahr contribute crucial information that could aid in delineating subsurface features, thus providing a more comprehensive understanding of the region's geological history and assisting in future planning and conservation efforts. Further analytical work, including the integration of geological mapping with geophysical data, is recommended to elucidate the complexities revealed by these surveys and enhance our scientific knowledge of these historically rich area.

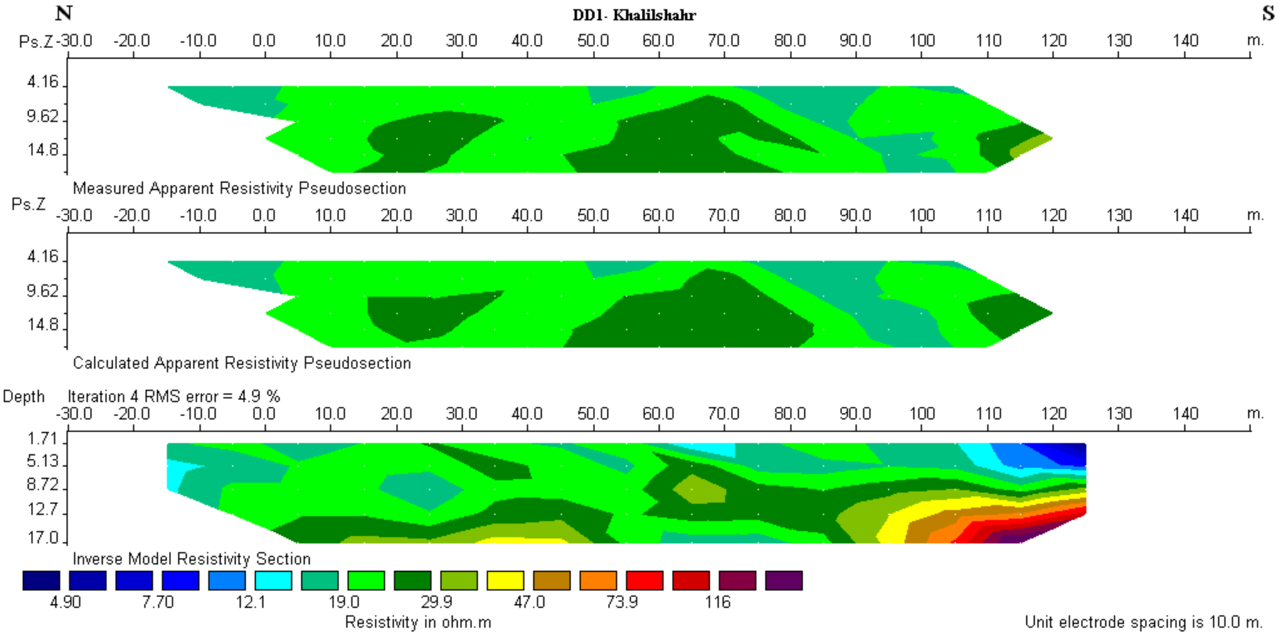

Figure 19: Apparent specific resistivity pseudo-sections with inverse model (Profile number 1, Khalil Shahr area

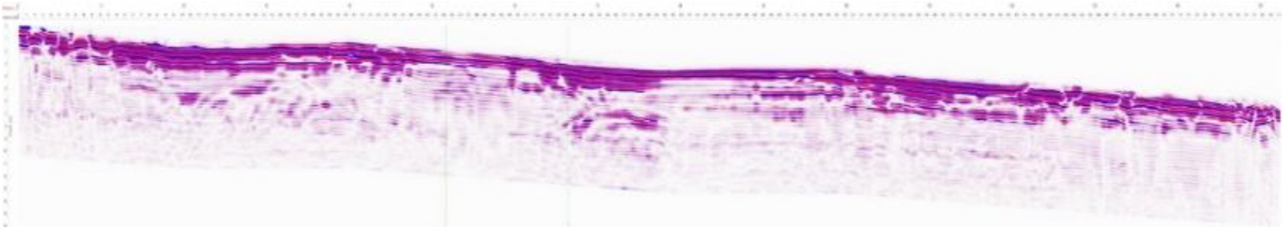

Figure 20: Depth section of profile number 1 using a 100 MHz cover antenna with topography

A schematic view, of a branch of the Caspian fault in Gohar Tappe site (Figure 21).

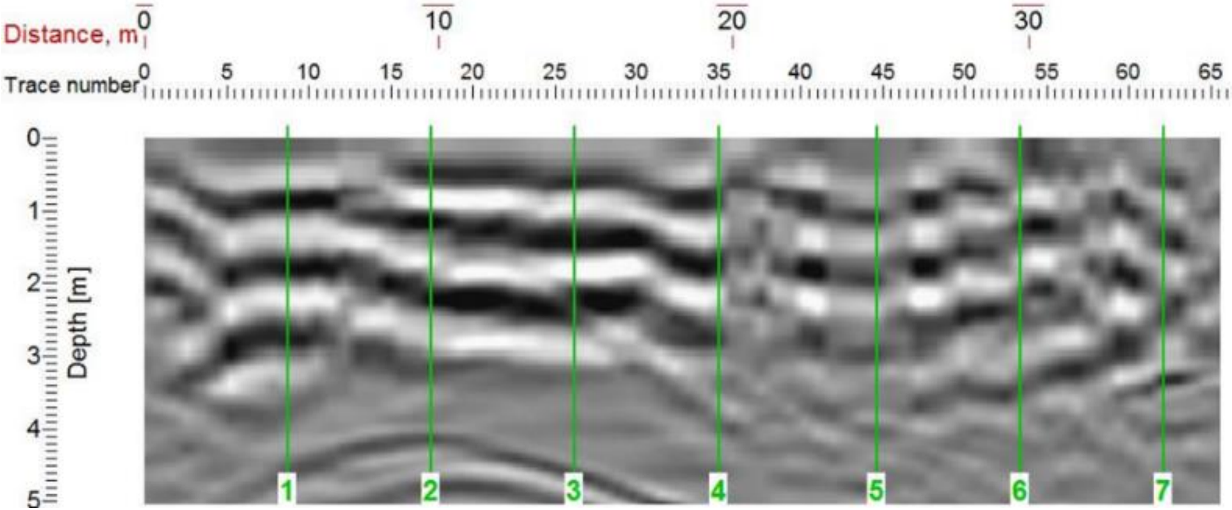

Figure 21: Depth section of profile number 2 using non-coated 100 MHz antenna (point to point)

References

Alahverdi Maygooni, F., Mohamadi Vizheh, M., Farrokhnia, A.R., Boostan, E., Nazari, H., 2019. Investigation of active tectonics and identification of active faults by geophysical methods case study: Gohartapeh- Behshahr. Scientific Quarterly Journal, Geosciences 28, 227–236 (In Persian).

Alavi, M., 1996. Tectonostratigraphic synthesis and structural style of the Alborz Mountain system in Northern Iran. J. Geodyn. 21 (1), 1–33.

Allen, M.B., Ghassemi, M.R., Shahrabi, M., Qorashi, M., 2003. Accommodation of late Cenozoic oblique shortening in the Alborz range, northern Iran. J. Struct. Geol. 25, 659–672.

Ambraseys, N.N., Melville, C.P., 1982. A history of Persian earthquakes. Cambridge University Press, New York, p. 219.

Antoine, P., Bahain, J.J., Berillon, G., Asgari Khaneghah, A., 2006. Tuf calcaire et se’quence alluvial en contexte tectonique actif : La formation de Baliran (province du Mazandaran, Iran). Quaternaire 17 (4), 321–331.

Bayasgalan, A., Jackson, J., Ritz, J.F., Carretier, S., 1999. Forebergs, flower structures, and the development of large intracontinental strike-slip faults: the Gurvan Bogd fault system in Mongolia. J. Struct. Geol. 21, 1285–1302.

Berberian, M., 1996. The Historical Earthquakes in Persia, pp. 635-640, http://www.iranicaonline.org/articles/earthquakes#iv.

Berberian, M., King, G., 1981. Towards a Paleogeography and tectonic evolution of Iran. Can. J. Earth Sci. 18 (2), 210–265.

Berberian, M., Qorashi, M., Jackson, J.A., Priestley, K., Wallace, T., 1992. The Rudbar-Tarom earthquake of 20 June 1990 in NW Persia - Prilimenary field and seismological observation, and its tectonic significance. Bull. Seismol. Soc. Am. 82 (4), 726–1755.

Brookfield, M.F., Hashmat, A., 2001. The geology and petroleum potential of the north Afghan platform and adjacent areas (northern Afghanestan, with parts of southern Turkmenistan, Uzbekistan and Tajikestan). Earth Scinces reviews 55, 41–71.

Brunet, M.F., Korotaev, M.V., Ershov, A.V., Nikishin, A.M., 2003. The South Caspian Basin: A review of its evolution from subsidence modelling. Sed. Geol. 156 (1–4), 119–148.

Djamour, Y., Vernant, P., Bayer, R., Nankali, H., Ritz, J.F., Hinderer, J., Hatam, Y.,Luck, B., Le Moigne, N., Sedighi, M., Khorrami, F., 2010. GPS and gravity constraints on continental deformation in the Alborz Mountain range. Iran, Geophysical Journal International 183, 1287–1301.

Dumoulin, J.P., Comby-Zerbino, C., Delqu´e-Koliˇc, E., Moreau, C., Caffy, I., Hain, S., Perron, M., Thellier, B., Setti, V., Berthier, B., Beck, L., 2017. Status report on sample preparation protocols developed at the LMC14 Laboratory, Saclay, France: from sample collection to 14C AMS measurement. Radiocarbon 59, 713–726.

Engdahl, E.R., Van der Hilst, R.D., Buland, R.P., 1998. Global teleseismic earthquake relocation with improved travel times and procedures for depth determination. Bull. Seismol. Soc. Am. 88, 772–1743.

Engdahl, E.R., Villase˜nor, A., 2002. Global Seismicity: 1900–1999, in W.H.K. Lee, H. Kanamori, P.C. Jennings, and C. Kisslinger (editors), International Handbook of Earthquake and Engineering Seismology, Part A, Chapter 41, pp. 665–690, Academic Press.

Gallardo, L.A., Meju, M.A., 2011. Structure-coupled Multiphysics imaging in geophysical sciences. RG1003, 1–19 Rev. Geophys. 49 (1). https://doi.org/10.10292010RG000330.

Ghassemi, M., 2005. Drainage evolution in response to fold growth in the hanging-wall of the Khazar fault, north-eastern Alborz. Iran. Basin Research 17, 425–436.

Ghassemi, M.R., Fattahi, M., Landgraf, A., Ahmadi, M., Ballato, P., Tabatabaei, S.H., 2014. Kinematic links between the Eastern Mosha Fault and the North Tehran Fault, Alborz range, northern Iran. Tectonophysics 622, 81–95.

Guest, B., Axen, G.J., Lam, P.S., Hassanzadeh, J., 2006. Late Cenozoic shortening in the west-central Alborz Mountains, northern Iran, by combined conjugate strike-slip and thin-skinned deformation. Geosphere 2 (1), 35–52.

Hollingworth, J., Jackson, J., Walker, R., Nazari, H., 2008. Extrusion tectonics and subduction in the eastern South Caspian region since 10 Ma. Geology 36 (10), 763–766.

Jackson, J., Priestley, K., Allen, M., Berberian, M., 2002. Active tectonics of the South Caspian Basin. Geophys. J. Int. 148, 214–245.

Javidfakhr, B., Bellier, O., Shabanian, E., Siame, L., Leanni, L., Bourles, D., Ahmadian, S., 2010. Fault kinematics and active tectonics at the southeastern boundary of the eastern Alborz (Abr and Khij fault zones): geodynamic implications for NNE Iran, Journal of Geodynamics, doi: 10.1016/j.jog.2011.02.005.

Loke, M.H., 2015. Tutorial: 2-D and 3-D electrical imaging surveys, www.geotomosoft.com, pp.169.

McCalpin, J., 2009. Paleoseismology, Volume 95, 2nd Edition, Elsiver, Paperback ISBN:9780123735768, eBook ISBN: 9780080919980, pp.629.

McKenzie, D.-P., 1972. Active tectonics of the Mediterranean region. Geophys. J. R.Astron. Soc. 30, 109–185.

Mohammadi Vizheh, M., Oskooi, B., Bastani, M., Kalscheuer, T., 2020. Using GPR Data as Constraints in RMT Data Inversion for Water Content Estimation: A Case Study in Heby, Sweden. Pure Appl. Geophys. 177 (6), 2903–2929. https://doi.org/10.1007/s00024-019-02391-1.

Moreau, C., Caffy, I., Comby, C., Delqu´e-Koliˇc, E., Dumoulin, J.-P., Hain, S., Quiles, A., Setti, V., Souprayen, C., Thellier, B., Vincent, J., 2013. Research and Development of the Artemis 14C AMS Facility: Status Report. Radiocarbon 55, 331–337.

Nabighian, M.N., 1991. Electromagnetic Methods in Applied Geophysics: Volume 2, Application, Parts A and B:

Volume 2, Application. Parts A and B. Society of Exploration Geophysicists.

Neal, A., 2004. Ground-penetrating radar and its use in sedimentology: principles, problems and progress. Earth Sci. Rev. 66 (3), 261–330.

Nazari, H., 2006. Analyse de la tectonique recente et active dans l'Alborz Central et la region de Teheran:Approche morphotectonique et paleoseismologique, Ph.D. thesis, Montpellier II, pp. 247, Montpellier- France.

Nazari, H., 2015. Analyse de la tectonique active en Iran : Approches morphotectonique at pal´ eosismologique : Implication en termes d'al´ ea sismique. G´ eosciences Montpellier, HDR thesis, Universit´ e Montpellier, Montpellier, France, pp :116.

Nazari, H., Ritz, J.F., Talebian, M., Moosavi, A., 2005. Seismotectonic map of the Central Alborz, Scale 1:250000, Geological Survey of Iran.

Nazari, H., Ritz, J.F., 2008. Neotectonics in Central Alborz. Geosciences, Geological Survey of Iran.special issue, 17 (1),74 -92.

Nazari, H., Ritz, J.F., Salamati, R., Shafei, A., Ghassemi, A., Michelot, J.L., Massault, M., Ghorashi, M., 2009. Morphological and Paleoseismological analysis along the Taleghan fault (Central Alborz, Iran). Geophys. J. Int. 178, 1028–1041.

Nazari, H., Ritz, J.F., Walker, R., Salamati, R., Rizza, M., Ghassemi, A., Patnaik, R., Hollingsworth, J., Alimohammadian, H., Jalali, A., Kaveh Firouz, A., Shahidi, A., 2014. Palaeoseismic evidence for a medieval earthquake, and prelimenary estimate of late Pliestocene slip-rate, on the Firouzkuh strike slip fault in the Central Alborz region of Iran. J. Asian Earth Sci. 82, 124–135.

Piller, C.K., Mahfroozi, A., 2009. First Prelimenary report on the joint Iranian-German excavations at Gohar Tappe, Mazandaran, Iran. 2100841 AMIT Band 41/2009, Stand vom: 19.3.2010, Trennprogr.: DeutschNeu, Satzprogramm: 3B2 insgesamt 34 Seiten, Verwendete Schrift: Meta (TrueType) — Registerhaltigkeit Grundschrift, u:/ p_1/ai/22ai_v2/007/22ai007.3d, Bearb.: Lier, pp. 33.

Prentice, C.S., Kendrick, K., Kelvin, B., Bayasgalan, A., Ritz, J.F., Spencer, J.Q., 2002. Prehistoric ruptures of the Gurvan Bulag fault, Gobi Altay, Mongolia. J. Geophys. Res. 107 (B12), 2321.https://doi.org/10.1029/2001JB000803.

Rashidi, A., 2021. Geometric and kinematic characteristics of the Khazar and North Alborz Faults: Links to the structural evolution of the North Alborz-South Caspian boundary. Northern Iran, Journal of Asian Earth Sciences 213. https://doi.org/10.1016/j.jseaes.2021.104755.

Ritz, J.F., Bourle‘s, D., Brown, E.T., Carretier, S., Chery, J., Enhtuvshin, B., Galsan, P., Finkel, R.C., Hanks, T.C., Kendrick, K.J., Philip, H., Raisbeck, G., Schlupp, A., Schwartz, D. P., Yiou, F., 2003. Late Pleistocene to Holocene slip rates for the Gurvan Bulag thrust fault (Gobi-Altay, Mongolia) estimated with 10Be dates, J. Geophys. Res., 108(B3), 2162, doi :10.1029/2001JB000553.

Ritz, J.F., Nazari, H., Ghassemi, A., Salamati, R., Shafei, A., Solaymani, S., Vernant, P., 2006. Active transtention inside Central Alborz: A new insight into the Northern Iran-Southern Caspian geodynamics. Geology 34 (6), 477–480.

Ritz, J.F., 2009. Extrusion tectonics and subduction in the eastern South Caspian region since 10 Ma: Comment: Geology.

Ritz, J.F., Nazari, H., Balescu, S., Lamothe, M., Salamati, R., Ghassemi, A., Shafei, A., Ghorashi, M., Saidi, A., 2012. Paleoearthquakes of the past 30000 years along the North Tehran Fault. Iran. Journal of Geophysical Research 117 (147), 1–15.

Rizza, M., Mahan, S., Ritz, J.-F., Nazari, H., Hollingsworth, J., Salamati, R., 2011. Using luminescence dating from coarse matrix material to estimate fault slip-rate in arid domain: Example of the Astaneh Fault (Iran). Quat. Geochronol. 6 (3–4), 390–406. https://doi.org/10.1016/j.quageo.2011.03.001.

Shahidi, A., 2008. Evolution tectonique du Nord de l’Iran (Alborz et Kopet-Dagh) depuis le M´ esozoïque. Ph.D. thesis, Universit´ e Pierre et Marie Curie, pp. 500, Paris, France.

Solaymani Azad, S., Ritz, J.F., Abbassi, M., 2011. Analysing the junction between the Mosha and the North Tehran active faults. Tectonophysics 497, 1–14. Stöcklin, J., 1974. Northern Iran: Alborz Mountains. Geological Society of London, Special publication 4, 213–234.

Talebian, M., Ghorashi, M., Nazari, H., 2013. Seismotectonic map of the Central Alborz, Scale 1:750000, Geological

Survey of Iran, http://ries.ac.ir/eqhazard/wp/Resualts.htm.

Talebian, M., Copley, A.C., Fattahi, M., Ghoraishi, M., Jackson, J.A., Nazari, H., Sloan, R. A., Walker, R.T., 2016. Active faulting within a megacity: the geometry and slip rate of the Pardisan thrust in central Tehran, Iran. Geophys. J. Int. 207 (3), 1688–1699. https://doi.org/10.1093/gji/ggw347.

Tatar, M., Jackson, J., Hatzfeld, D., Bergman, E., 2007. The 28 May 2004 Baladeh earthquake (Mw 6.2) in the Alborz, Iran: overthrusting the South Caspian Basin margin, partitioning of oblique convergence, and the seismic hazard of Tehran. Geophys. J. Int. 170, 249–261.

Vernant, P., Nilforoushan, F., Chery, J., Bayer, R., Djamour, Y., Masson, F., Nankali, H., Ritz, J.F., Sedighi, M., Tavakoli, F., 2004. Deciphering oblique shortening of central Alborz in Iran using geodetic data. Earth Planet. Sci. Lett. 223, 177–185.

Walker, R.T., Jackson, J., Baker, C., 2003. Surface expression of thrust faulting in eastern Iran: Source parameters and surface deformation of the 1978 Tabas and 1968 Ferdows earthquake sequences. Geophys. J. Int. 152, 749–765. https://doi.org/10.1046/j.1365-246X.2003.01886.x.

Wells, D.L., Coppersmith, K.J., 1994. Empirical relationships among magnitude, rupture lenght, rupture area, and surface displacement. Bull. Seismo. Soc. Am. 84, 974–1002.